

Light quark energy loss in strongly-coupled $\mathcal{N} = 4$ supersymmetric Yang-Mills plasma

Paul M. Chesler*, Kristan Jensen†, Andreas Karch‡, and Laurence G. Yaffe§

Department of Physics, University of Washington, Seattle, WA 98195, USA

(Dated: October 29, 2018)

We compute the penetration depth of a light quark moving through a large N_c , strongly coupled $\mathcal{N} = 4$ supersymmetric Yang-Mills plasma using gauge/gravity duality and a combination of analytic and numerical techniques. We find that the maximum distance a quark with energy E can travel through a plasma is given by $\Delta x_{\max}(E) = (\mathcal{C}/T) (E/T\sqrt{\lambda})^{1/3}$ with $\mathcal{C} \approx 0.5$.

I. INTRODUCTION

The discovery that the quark-gluon plasma produced at RHIC behaves as a nearly ideal fluid [1, 2] has prompted much interest into the dynamics of strongly coupled plasmas. Hard partons produced in the early stages of heavy ion collisions can traverse the resulting fireball and deposit their energy and momentum into the medium. Analysis of particle correlations in produced jets can provide useful information about the dynamics of the plasma including the rates of energy loss and momentum broadening [3, 4], as well as the speed and attenuation length of sound waves [4].

Gauge/gravity duality [5, 6, 7, 8] is a useful tool for the study of dynamics of strongly coupled non-Abelian plasmas. Although no gravitational dual to QCD is known, gauge/gravity duality has provided much insight into the dynamics of various theories which share many qualitative properties with QCD. The most widely studied example is that of strongly coupled $\mathcal{N} = 4$ supersymmetric Yang-Mills theory (SYM). The deconfined plasma phases of QCD and SYM share many properties. For example, both theories describe non-Abelian plasmas with Debye screening, finite spatial correlation lengths, and long distance dynamics described by neutral fluid hydrodynamics. When both theories are weakly coupled, appropriate comparisons of a variety of observables show rather good agreement [9, 10, 11]. This success, combined with the lack of alternative techniques for studying dynamical properties of QCD at temperatures where the plasma is strongly coupled, has motivated much interest in using strongly coupled $\mathcal{N} = 4$ SYM plasma as a model for QCD plasma at temperatures of a few times Λ_{QCD} (or $1.5 T_c \lesssim T \lesssim 4 T_c$). (See, for example, Refs. [12, 13, 14, 15, 16, 17, 18, 19, 20, 21, 22, 23, 24, 25], and references therein.) At least for some quantities, this is quite successful. In particular, the value of the shear viscosity to entropy density ratio [12, 26], $\eta/s = 1/4\pi$, in strongly coupled SYM is in rather good agreement with estimates which emerge from hydrodynamic modeling of heavy ion collisions [27].

In the limit of large N_c and large 't Hooft coupling $\lambda \equiv g^2 N_c$, the gravitational dual to $\mathcal{N} = 4$ SYM is described by classical supergravity on the ten dimensional $AdS_5 \times S^5$ geometry [5]. Studying the theory at finite temperature corresponds to adding a black hole to the geometry [6]. The corresponding AdS-Schwarzschild (AdS-BH) metric is given below in Eq. (2.1). Fundamental representation quarks added to the $\mathcal{N} = 4$ theory are dual to open strings moving in the $10d$ geometry. In the limit of large λ , where the string action and the energy both scale like $\sqrt{\lambda}$, quantum fluctuations in the string worldsheet are suppressed and the dynamics of strings may be described by the classical equations of motion which follow from the Nambu-Goto action.

The dynamics of strings corresponding to heavy quarks have been intensely studied by many authors. The energy loss rate for heavy quarks moving through a SYM plasma has been studied in Refs [13, 14, 28, 29], and the wake produced by a moving heavy quark was computed in Refs. [30, 31, 32, 33].

Analogous studies for light quarks have yet to be completed. In Ref. [34] the charge density of massless quarks moving through a SYM plasma was studied, and it was shown that there are string states which are dual to long-lived excitations (*i.e.*, quasi-particles) in the field theory. In particular, the charge density of highly energetic light quarks can remain localized for an arbitrarily long time, and can propagate arbitrarily far before spreading out and thermalizing. In Ref. [35], an attempt was made to estimate the penetration depth of a gluon moving through a strongly coupled SYM plasma. The results of Ref. [35] were obtained by assuming that the endpoint of a (folded) string follows a light-like geodesic in the AdS-BH geometry; full solutions to the string equations of motion were not obtained. The authors of Ref. [35] tried to roughly characterize the relationship between the string's energy and momentum and the parameters of the geodesic, and suggested that the maximum distance a gluon of energy E can go before thermalizing should scale as $\Delta x_{\max} \sim E^{1/3}$. The same scaling relation has also been discussed for R -current jets in Ref. [36].

Although the estimates made in Ref. [35] are generally plausible, we believe that it is clearly desirable to perform a quantitative, controlled study of the penetration distance of light quarks (or gluons) in a strongly coupled plasma. This is a key aim of this paper.

It should be emphasized that we are concerned with

* Email: pchesler@u.washington.edu

† Email: kristanj@u.washington.edu

‡ Email: karch@phys.washington.edu

§ Email: yaffe@phys.washington.edu

studying the propagation through the plasma of energetic excitations which resemble well-collimated quark jets. The open string configurations we consider may be regarded as providing a dual description of dressed quarks, with high energy, moving through a non-Abelian plasma. We are not studying the result of a local current operator acting directly on the strongly coupled $\mathcal{N}=4$ SYM plasma. (See, however, Ref. [37].) Our motivation is similar to that of Ref. [17], in which weak coupling physics in asymptotically free QCD is envisioned as producing a high energy excitation, whose propagation through the plasma is then modeled by studying the behavior of the same type of excitation in a strongly coupled $\mathcal{N}=4$ SYM plasma.

The energy loss rate for a heavy quark depends only on the quark's velocity, the value of the 't Hooft coupling λ , and the temperature of the plasma through which the quark is moving [13]. In other words, for very heavy quarks which slowly decelerate, the velocity is the only aspect of their initial conditions which influences the energy loss rate. This turns out not to be the case for light quarks. Initial conditions for a classical string involve two free functions: the initial string profile and its time derivative. As we discuss in detail below, the instantaneous energy loss rate of a light quark depends strongly, in general, on the precise choice of these initial functions. In the dual field theory, this reflects the fact that any complete specification of an initial state containing an energetic quark must also involve a characterization of the gauge field configuration. In the perturbative regime, one can easily see that the interactions of heavy particles with a gauge field are spin-independent (up to $1/M$ corrections), but interactions of relativistic particles are spin-dependent even at leading order. So it is perhaps unsurprising that the energy loss of a light projectile also depends on the configuration of the gluonic cloud surrounding the projectile in a non-universal fashion.

One quantity which is rather insensitive to the precise initial conditions of the string is the maximum distance $\Delta x_{\max}(E)$ which a quark with initial energy E can travel. It should be emphasized that we are considering effectively on-shell quarks which can travel a large distance Δx before thermalizing. The maximum penetration depth Δx_{\max} grows without bound as the energy E increases.

We numerically compute the penetration depth Δx for many different sets of string initial conditions, and find that the maximum penetration depth does indeed scale like $E^{1/3}$. Our results are illustrated in Fig. 1, where the logarithm of the penetration depth is plotted as a function of the logarithm of the initial quark energy for many different sets of initial conditions. As is evident from the figure, the penetration depth of a light quark is bounded by a curve $\Delta x_{\max} = \text{const.} \times E^{1/3}$.

We also demonstrate the scaling relation $\Delta x_{\max} \sim E^{1/3}$ analytically. As discussed in Ref. [34], strings which correspond to long-lived massless quarks are approxi-

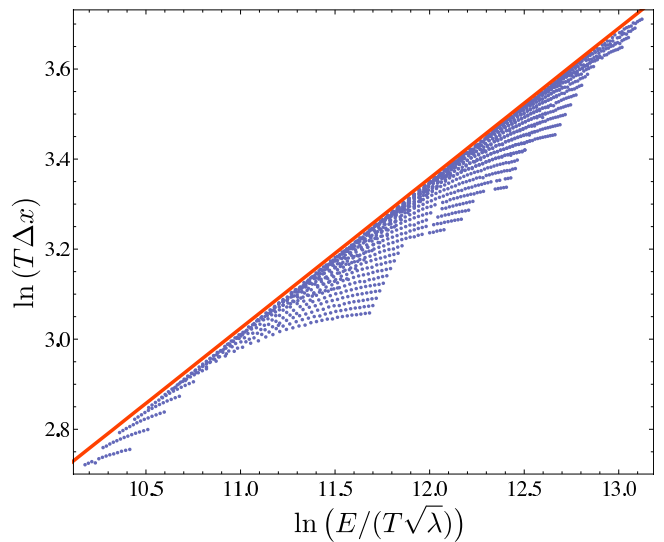


FIG. 1: A log-log plot of the quark stopping distance Δx as a function of total quark energy E for many falling strings with initial conditions of the form shown in Eq. (4.53). All data points fall below the red line given by $\Delta x = (0.526/T)(E/T\sqrt{\lambda})^{1/3}$.

mately null strings. A strictly null string is one whose worldsheet metric is everywhere degenerate. The qualitative origin of this connection is easy to understand. Strings which correspond to light quarks fall into the event horizon. As they fall they become more and more light-like and hence closer and closer to a null configuration as time progresses. The profile of the null string is almost independent of the initial conditions used to create the string — for the quasiparticle excitations studied in this paper, the corresponding null strings are specified by two numbers only, an initial inclination and radial depth. By analyzing strings corresponding to light quarks as small perturbations away from null string configurations, we show that the total distance a quark can travel must be bounded by a maximum distance $\Delta x_{\max} = (\mathcal{C}/T)(E/T\sqrt{\lambda})^{1/3}$ for some $O(1)$ constant \mathcal{C} . We numerically confirm that strings corresponding to long-lived light quarks are, in fact, close to being null, and obtain an estimate of the constant \mathcal{C} .

Although the endpoint motion of our string solutions is well approximated by appropriate light-like geodesics, consistent with the discussion of Ref. [34], we find that the relationship between the parameters of the geodesic and the string profile and energy is more complicated (and rather different) than the surmises presented in Ref. [35]. This will be discussed further in Section V.

In addition to studying the penetration depth, we also examine the instantaneous rate of energy loss, dE/dt . For light quarks the energy loss rate shows non-universal features and is sensitive to initial conditions. For the states we study, we find that it typically *increases* with time during the period when the dressed quark is a well-defined quasiparticle and sharply peaks during the final

thermalization phase. In other words, the thermalization of light quarks in strongly coupled SYM ends with an explosive burst of energy. This late time behavior is universal and independent of initial conditions. The fact that the light quark energy loss rate can increase with time is qualitatively different from the behavior of heavy particles [13], whose energy loss rate monotonically decreases.

An outline of our paper is as follows. We define our conventions in Section II. In Section III, we discuss some of the subtleties involved in defining the light quark energy loss rate and penetration depth, and spell out the relevant identifications between $5d$ gravitational and $4d$ field theory quantities. In Section IV, we discuss the dynamics of strings both from analytical and numerical perspectives. Implications of our results, and connections with other related work, are discussed in Section V, which is followed by a brief conclusion.

II. CONVENTIONS

Five dimensional AdS coordinates will be denoted by X_M , while four dimensional Minkowski coordinates are denoted by x_μ . Worldsheet coordinates will be denoted as σ^a with $a = 0, 1$. The timelike world sheet coordinate is $\tau \equiv \sigma^0$, while the spatial coordinate is $\sigma \equiv \sigma^1$. When discussing the dynamics of a single string endpoint, we will use σ^* to denote the value of σ at the endpoint.

We choose coordinates such that the metric of the AdS-Schwarzschild (AdS-BH) geometry is

$$ds^2 = \frac{L^2}{u^2} \left[-f(u) dt^2 + d\mathbf{x}^2 + \frac{du^2}{f(u)} \right], \quad (2.1)$$

where $f(u) \equiv 1 - (u/u_h)^4$ and L is the AdS curvature radius. The coordinate u is an inverse radial coordinate; the boundary of the AdS-BH spacetime is at $u = 0$ and the event horizon is located at $u = u_h$, with $T \equiv (\pi u_h)^{-1}$ the temperature of the equilibrium SYM plasma.

III. LIGHT QUARKS AND GAUGE/GRAVITY DUALITY

Energetic quarks moving through a plasma are quasi-particles — they have a finite lifetime which can be long compared to the inverse of their energy. Some care is needed in defining the light quark penetration depth and the instantaneous energy loss rate. Fig. 2 shows some typical perturbative diagrams contributing to the energy loss rate of a quark. A energetic quark, scattering off excitations in the medium, can emit gluons which may subsequently split into further gluons or quark-antiquark pairs. The energetic quark may also annihilate with an antiquark in the medium. A natural question to consider when looking at Fig. 2 is which quark should one follow when computing the penetration depth? Once a quark

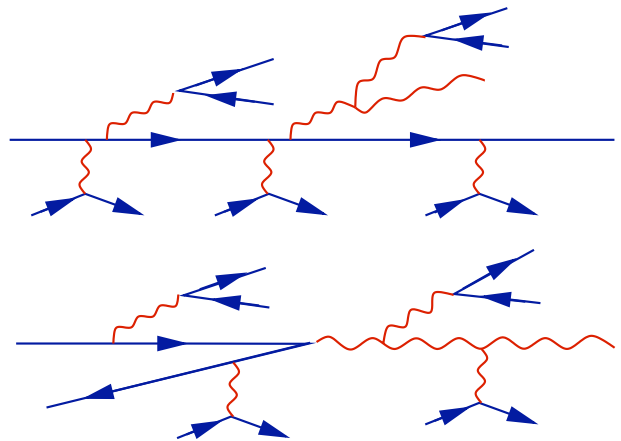


FIG. 2: Examples of perturbative diagrams contributing to the energy loss of a quark. One may regard time as running to the right. An energetic quark can scatter, emit gluons (which themselves may radiate or split into $q\bar{q}$ pairs), or annihilate with an antiquark in the medium. However, the total baryon number of the state remains constant.

has emitted a $q\bar{q}$ pair, or annihilated with an antiquark, it becomes ambiguous which quark was the original one. This issue is cleanly avoided if one focuses attention not on some (ill-defined) “bare quark”, but rather on the baryon density of the entire dressed excitation.

In QCD, or $\mathcal{N} = 4$ SYM coupled to a fundamental representation $\mathcal{N} = 2$ hypermultiplet, there is a conserved current which we will call J_{baryon}^μ . Even though $q\bar{q}$ pairs can be produced by an energetic quark traversing the plasma, conservation of J_{baryon}^μ implies that the total baryon number of the excitation will remain constant. The baryon density of an energetic excitation can remain highly localized for a long period of time. It is the collective excitation with localized baryon density which we will refer to as a dressed quark, or for the sake of brevity, simply as a quark.

To evaluate the penetration depth of a quark, we will use the centroid of the baryon density,

$$\bar{\mathbf{x}}(t) \equiv \frac{\int d^3x \mathbf{x} \rho(t, \mathbf{x})}{\int d^3x \rho(t, \mathbf{x})}. \quad (3.1)$$

with $\rho \equiv J_{\text{baryon}}^0$. The centroid $\bar{\mathbf{x}}(t)$ gives a natural measure of where the quark is located at time t . At late times, when the quark has lost nearly all its energy and becomes thermalized, the dynamics of the baryon density will be governed by hydrodynamics. In particular, at late times the baryon density must satisfy the diffusion equation

$$(\partial_0 - D\nabla^2) \rho = 0, \quad (3.2)$$

where D is the baryon number diffusion constant. When the diffusion equation is applicable, it is easy to see that the centroid ceases to move, $d\bar{\mathbf{x}}/dt = 0$. To define the penetration depth, we imagine measuring $\bar{\mathbf{x}}(t)$ at some

early time t_* . We then define the penetration depth Δx in the obvious manner as

$$\Delta x \equiv |\bar{x}(\infty) - \bar{x}(t_*)|. \quad (3.3)$$

On the gravitational side of the gauge/gravity correspondence, the addition of a $\mathcal{N}=2$ hypermultiplet to the $\mathcal{N}=4$ SYM theory is accomplished by adding a $D7$ brane to the $10d$ geometry [38]. The $D7$ brane fills a volume of the AdS-BH geometry which extends from the boundary at $u=0$ down to maximal radial coordinate u_m , and wraps an S^3 of the S^5 . The bare mass M of the hypermultiplet is proportional to $1/u_m$ [13], so for massless quarks the $D7$ brane fills all of the five-dimensional AdS-BH geometry. Open strings which end on the $D7$ brane represent *dressed* $q\bar{q}$ pairs in the field theory. In the $5d$ geometry these strings can fall unimpeded toward the event horizon until their endpoints reach the radial coordinate u_m where the $D7$ brane ends.¹ For sufficiently light or massless quarks, $u_m > u_h$ and open string endpoints can fall into the horizon.²

The endpoints of strings are charged under a $U(1)$ gauge field \mathcal{A}_M which resides on the $D7$ brane. The boundary of the $5d$ geometry, which is where the field theory lives, behaves as an ideal electromagnetic conductor [39] and hence the presence of the string endpoints, which source the $D7$ gauge field \mathcal{A}_M , induce an *image current density* J_{baryon}^μ on the boundary. This is illustrated schematically by the cartoon in Fig. 3. Via the standard gauge/gravity dictionary [5, 6, 7, 8, 38], the induced current density corresponding to each string

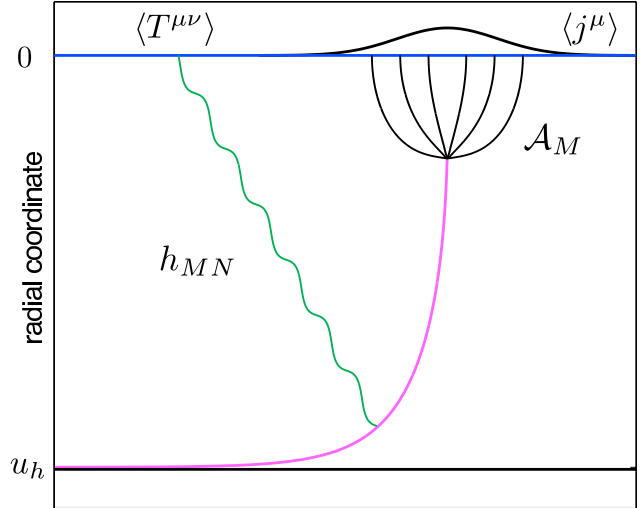


FIG. 3: A cartoon of the bulk-to-boundary problem at finite temperature. The endpoints of strings are charged under a $U(1)$ gauge field \mathcal{A}_M which lives on the $D7$ brane which fills the AdS-BH geometry. The boundary of the geometry, located at radial coordinate $u=0$, behaves like a perfect conductor. Consequently, the string endpoints induce a mirror current density j^μ on the boundary. Via gauge/gravity duality, the induced mirror current density has the interpretation of minus the baryon current density of a quark. Similarly, the presence of the string induces a perturbation h_{MN} in the metric of the bulk geometry. The behavior of the metric perturbation near the boundary encodes the information contained in the perturbation to the SYM stress-energy tensor caused by the presence of the jet.

¹ One should bear in mind that even when the radial position of the string endpoints lies closer to the boundary than u_m , the string endpoints are nevertheless attached to the $D7$ brane, albeit in the full $10d$ space. The embedding of the $D7$ brane is determined dynamically by minimizing the $D7$ worldvolume. In general, this means that the $D7$ brane wraps a 3-sphere inside the S^5 of the AdS-BH $\times S^5$ background geometry. This 3-sphere varies in a non-trivial way as a function of the radial coordinate of the AdS-BH geometry. For a hypermultiplet with non-zero mass, the string endpoints must move on the internal S^5 as they fall down in the AdS-BH geometry, so that the string endpoints remain on the $D7$ brane. But for massless hypermultiplets, the corresponding $D7$ embedding is a simple product space, AdS-BH $\times S^3$. In this case, it is consistent to have the entire string sit at a fixed point on the S^5 while it falls in the AdS-BH background. Any additional motion of the string in the internal space will only add to the energy of the string without affecting its stopping distance and so will be of no interest for us — we want to find strings which carry a minimal amount of energy for a given stopping distance. In the large N_c limit, one can ignore the backreaction of the $D7$ brane on the background geometry and the backreaction of the string on the $D7$, as well as potential instabilities involving string breaking or dissolving into the D-brane. These issues are discussed further in Section V.

² Strictly speaking, in the coordinate system we are using no portion of the string crosses the horizon at any finite value of time. Due to the gravitational redshift, the rate of fall du/dt decreases exponentially as one approaches the horizon. Nevertheless, it is natural to speak of the string endpoint falling “into” or “reaching” the horizon when $u - u_h \ll u_h$.

endpoint has a field theory interpretation as minus the baryon current density of a dressed quark.³

The degree to which the baryon density is localized depends on how close the string endpoint is to the boundary of the $5d$ geometry. The farther the endpoint is away from the boundary, the more the field lines of \mathcal{A}_M can spread out, and hence the more delocalized will be the induced image current J_{baryon}^μ . In the limit where the radial coordinate \mathcal{U} of the string endpoint is far from the horizon, $\mathcal{U} \ll u_h$, the baryon density will be localized with a length scale $\sim \mathcal{U}$ [34]. We note that the appearance of the length scale \mathcal{U} in the baryon density is natural since, for $\mathcal{U} \ll u_h$, it takes light an amount of time $\sim \mathcal{U}$

³ The fact that the induced mirror current density is minus the physical baryon current density is easy to understand. The baryon current density is given by the variation of the on-shell electromagnetic action with respect to the boundary value of the gauge field \mathcal{A}_M . The on-shell $5d$ electromagnetic action evaluates to a $4d$ surface integral, evaluated at the boundary with an outward pointing normal. In contrast, the image current density induced on the boundary can be obtained by integrating the $5d$ Maxwell equations over a Gaussian pillbox which encloses the boundary. The resulting surface integral measuring the flux involves an inward pointing normal (*i.e.*, into the $5d$ bulk).

to reach the boundary.

If at time t_* the string's endpoint is at radial coordinate $u_* \ll u_h$, then $\bar{\mathbf{x}}(t_*)$ approximately coincides with the spatial position of the string endpoint $\mathbf{x}_{\text{string}}(t_*)$ [34]. The string endpoint can only travel a finite distance before falling into the black hole. The final spatial coordinate of the string endpoint $\mathbf{x}_{\text{string}}(\infty)$ will exactly coincide with $\bar{\mathbf{x}}(\infty)$ [34]. We therefore have

$$\Delta x \approx |\mathbf{x}_{\text{string}}(\infty) - \mathbf{x}_{\text{string}}(t_*)|. \quad (3.4)$$

To make the quantity $\Delta x_{\text{max}}(E)$ meaningful, we also need to measure the quark's energy at time t_* . After all, we want to know how far a quark with a given initial energy can travel. If the quark has been moving for some time prior to t_* , it will have deposited energy into the plasma — we must disentangle the energy deposited in the plasma from the remaining energy of the quark itself. In the limit where the quark has an arbitrarily large energy which is localized in a arbitrarily small region of space, separating the quark's energy from the energy transferred to the plasma will be unambiguous.

Via Einstein's equations, the presence of the string will also perturb the $5d$ geometry. As in the electromagnetic problem, the perturbation in the geometry will induce a corresponding perturbation in the $4d$ stress tensor on the boundary [40, 41]. The string itself has a conserved energy. For the states we consider in this paper, the endpoints of the string are very close to the boundary at time t_* and hence have a very high gravitational potential energy. In Section IV A we argue that the energy contained near a string endpoint scales like $1/u_*^3$. It is this *UV sensitive* part of the string energy that we identify with the energy of a quark. Via the gravitational bulk-to-boundary problem [also illustrated in the cartoon of Fig. (3)] the high energy density near the string endpoint gets mapped onto a region of $4d$ space which coincides with the location of the quark's baryon density. Therefore, at time t_* , we only need to compute the part of the string's energy which diverges in the $u_* \rightarrow 0$ limit in order to identify the energy of the corresponding quark.

IV. FALLING STRINGS

The dynamics of a classical string are governed by the Nambu-Goto action

$$S_{\text{NG}} = -T_0 \int d\tau d\sigma \sqrt{-\gamma}, \quad (4.1)$$

where $T_0 = \sqrt{\lambda}/(2\pi L^2)$ is the string tension, σ and τ are worldsheet coordinates, and $\gamma \equiv \det \gamma_{ab}$ with γ_{ab} the induced worldsheet metric. The string profile is determined by a set of embedding functions $X^M(\tau, \sigma)$. In terms of these functions

$$\gamma_{ab} = \partial_a X \cdot \partial_b X, \quad (4.2)$$

and

$$-\gamma = (\dot{X} \cdot X')^2 - \dot{X}^2 X'^2, \quad (4.3)$$

where $\dot{X}^M \equiv \partial_\tau X^M$ and $X'^M \equiv \partial_\sigma X^M$.

The equations of motion for the embedding functions, as well as the requisite open string boundary conditions, follow from demanding vanishing variation of the Nambu-Goto action. Explicit forms of the resulting equations of motion, for the class of configurations we will consider, are shown below in Section IV A. The boundary conditions for the open string require that its endpoints move at the local speed of light and that their motion is transverse to the string.

We will limit attention to configurations for which the string embedding only has non-zero components along a single Minkowski spatial direction which we will denote as \hat{x} . We also restrict attention to initial conditions such that at worldsheet time $\tau = 0$, the string is mapped into a single point in spacetime. Explicitly,

$$t(0, \sigma) = t_c, \quad x(0, \sigma) = x_c, \quad u(0, \sigma) = u_c, \quad (4.4)$$

where the numbers t_c , x_c , and u_c specify the $5d$ space-time location of the string creation event. The remaining initial data are the velocity profiles at $\tau = 0$, namely \dot{t} , \dot{x} and \dot{u} as functions of σ . One of these three velocity functions may be eliminated via gauge fixing. For example one may choose the gauge $\tau = t$.

We will be interested in choosing initial data such that the subsequent evolution leads to configurations in which the two string endpoints propagate away from each other and become well separated before falling into the horizon. Choosing a frame in which the total spatial momentum of the string vanishes, this implies that one half of the string will carry a large positive spatial momentum in the \hat{x} direction, while the other half carries a large negative spatial momentum. We also require that the velocity profiles are smooth near the string endpoints. A sufficient condition is that the Fourier series of the velocity profiles be rapidly convergent (pointwise). For brevity, we will refer to string configurations satisfying these conditions as “reasonable”. We postpone more detailed discussion of our specific choices of velocity profiles used for numerical studies to Section IV B.

A. Approximate solutions

Consider a string created in the distant past. In particular, take the radial coordinate of the creation event to be arbitrarily small, $u_c \rightarrow 0$. As time progresses, the string evolves from a point into an extended object and the endpoints of the string fall toward the horizon. An example of such string evolution (numerically computed) is shown in Fig. 4. As we discuss in detail below, in the limit $u_c \rightarrow 0$, the string endpoints can be made to travel arbitrarily far in the spatial \hat{x} direction before falling into

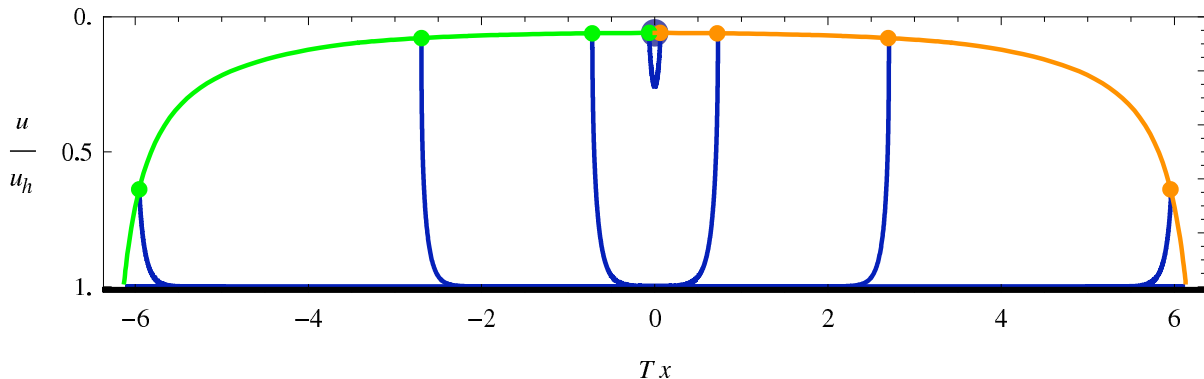


FIG. 4: A typical falling string studied in this paper, plotted in blue at four different instants in time. The string is created at a point and, as time passes, evolves into an increasingly extended object. Well after the creation event, but long before the plunge into the horizon, the string profile approaches a universal *null string* configuration which is largely insensitive to the initial conditions. Consequently, the string endpoint trajectories, shown in green and yellow, approach null geodesics.

the black hole. Our strategy in this subsection is to construct an approximate solution to the string equations of motion which will provide a good description for times sufficiently long after the initial creation event but well before the string endpoints reach the horizon. This will be possible because, as we will discuss, at times well after the creation event but long before the final “plunge”, typical string configurations approach near-universal forms which are characterized by only a few parameters. This observation will allow us to prepare states illustrating universal features and understand the resulting physics of quark energy loss, without requiring a detailed description of the early-time dynamics responsible for the production of the quark-antiquark pair.

For reasonable falling string solutions, we will see that the endpoint motion is well-approximated by the trajectory of a light-like geodesic. Equations for null geodesics in the AdS-BH geometry are easy work out. For motion in the x - u plane, one finds

$$\left(\frac{dx_{\text{geo}}}{dt}\right)^2 = \frac{f^2}{\xi^2}, \quad (4.5a)$$

$$\left(\frac{du_{\text{geo}}}{dt}\right)^2 = \frac{f^2(\xi^2 - f)}{\xi^2}, \quad (4.5b)$$

where ξ is a constant which determines the initial inclination of the geodesic in the x - u plane and, more fundamentally, specifies the conserved spatial momentum associated with the geodesic, $f(u)^{-1}dx_{\text{geo}}/dt = \xi^{-1}$. Moreover, we have

$$\left(\frac{dx_{\text{geo}}}{du}\right)^2 = \frac{1}{\xi^2 - f}. \quad (4.6)$$

From this equation, one sees that geodesics which start close to the boundary, at $u = u_* \rightarrow 0$, can travel very far in the \hat{x} direction provided $\xi^2 \approx f(u_*) \rightarrow 1$. In particular, the total spatial distance such geodesics travel before falling into the horizon scales like u_h^2/u_* .

We will be interested in string configurations where the spatial velocity of the string endpoint is close to the local speed of light for an arbitrarily long period of time (since this will maximize the penetration distance). Because open string endpoints must always travel at the speed of light, the velocity in the radial direction must be small and correspondingly, the radial coordinate of the string endpoints will be approximately constant for an arbitrarily long period of time. As the string endpoints become more and more widely separated, the string must stretch and expand. For reasonable string profiles, this implies that short wavelength perturbations in the initial structure of the string will stretched to progressively longer wavelengths, resulting in a smooth string profile at late times.⁴ Moreover, as the string endpoints separate, the middle of the string must fall toward the event horizon. This occurs on a time scale Δt of order u_h . (This scale sets the infall time of a particle released at rest at the boundary, or of a null geodesic with $\xi > 1$.)

The origin of this behavior can also be understood as follows. Consider the string at some time t shortly after the creation event. It will have expanded to a size $\sim t$. By construction, one half of the string will have a positive large momentum in the spatial \hat{x} direction, while the other half has negative \hat{x} momentum. The spatial momentum density must be highly inhomogeneous so that the two endpoints move off in opposite directions. As time progresses, the parts of the string with the highest momentum density will remain close to a string endpoint. Portions of the string with low spatial momentum den-

⁴ “Unreasonable” string profiles can have structure on arbitrarily short wavelengths. While the initial structure will be inflated as time progresses, because the string endpoints can only travel a distance of order u_h^2/u_c before reaching the horizon, one can always cook up initial conditions such that fluctuations in the string profile never become small during this time interval. We will avoid such unreasonable initial conditions in this paper.

sity will lag behind the endpoints (in terms of motion in the \hat{x} direction) and fall relatively unimpeded toward the horizon. Thereafter, the outer parts of the string will continue moving in the $\pm\hat{x}$ direction while the endpoints slowly fall. This general behavior is clearly seen in Fig. 4.

With the above qualitative picture in mind, we now turn to the explicit analysis. To simplify the discussion, focus attention on one half of the string. We may choose worldsheet coordinates $\tau = t$ and $\sigma = u$, so that the embedding functions are determined by a single function $x(t, u)$. The domain in the (t, u) plane in which $x(t, u)$ is defined is bounded by a curve $\mathcal{U}(t)$ which defines the trajectory of the string endpoint. The location of this curve is fixed by the open string boundary conditions. With our choice of worldsheet coordinates, these boundary conditions are simply

$$G_{MN} \frac{dX^M}{dt} \frac{dX^N}{dt} = 0, \quad (4.7a)$$

$$G_{MN} \frac{dX^M}{dt} \frac{\partial X^N}{\partial u} = 0, \quad (4.7b)$$

where the total time derivatives denote derivatives evaluated along the curve $\mathcal{U}(t)$. As noted earlier, these conditions just express the constraints that the speed of the string endpoint equal the local speed of light with a velocity which is transverse to the string.

With our choice of worldsheet coordinates, the determinant of the worldsheet metric is

$$\gamma = \frac{L^4}{u^4 f} (f^2 x'^2 - \dot{x}^2 + f). \quad (4.8)$$

Substituting this into the Nambu-Goto action (4.1), one finds the following equation of motion for the embedding function $x(t, u)$,

$$0 = 2u(1 + f x'^2) \ddot{x} - 2uf(f - \dot{x}^2) x'' - 4ufx' \dot{x}' + 4f[2 - f(1 - x'^2)] x' - 4(3 - 2f)x' \dot{x}^2. \quad (4.9)$$

We want to construct an approximate solution for configurations where the string endpoint reaches the event horizon after traveling an arbitrarily large spatial distance. We imagine first matching our approximate solution onto an exact string solution at a time t_* . At time t_* , suppose that one endpoint of the string has fallen to the radial coordinate u_* . Because we are considering $u_c \rightarrow 0$, we can always take

$$u_c \ll u_* \ll u_h. \quad (4.10)$$

For reasonable initial conditions, we can take t_* sufficiently large so that the string will be close to a quasi-stationary configuration in which the string profile uniformly translates while the string endpoint slowly falls. In other words, we seek a perturbative solution to Eq. (4.9) of the form

$$x(t, u) = x_{\text{steady}}(t, u) + \delta x(t, u) + O((\delta x)^2), \quad (4.11)$$

where

$$x_{\text{steady}}(t, u) = \xi t + x_0(u) \quad (4.12)$$

is a stationary solution to the equations of motion (4.9) and $\delta x(t, u)$ is a first order perturbation satisfying

$$|\delta \dot{x}(t, u)| \ll \xi, \quad |\delta x(t, u)| \ll |x_0(u)|, \quad (4.13)$$

for all $t > t_*$ and all $u > \mathcal{U}(t)$.

At this point, the constant ξ appearing in the stationary solution x_{steady} is logically independent from the parameter ξ characterizing null geodesics [c.f. Eq. (4.5)], but we will shortly see that the endpoint trajectory of the stationary solution x_{steady} is in fact directly related to the null geodesics discussed above.

The endpoint trajectory may similarly be represented as a zeroth order curve plus a first order correction,

$$\mathcal{U}(t) = \mathcal{U}_0(t) + \delta \mathcal{U}(t), \quad (4.14)$$

where $\mathcal{U}_0(t)$ is the endpoint trajectory when $\delta x(t, u) = 0$.

The function $\delta x(t, u)$ characterizes the perturbations in the string which have inflated to long wavelengths. Our basic strategy is to linearize the equations of motion and boundary conditions in both $\delta x(t, u)$ and $\delta \mathcal{U}(t)$. From Eq. (4.9), the equation of motion for $x_0(u)$ is

$$0 = 2uf(\xi^2 - f)x_0'' + 4f^2x_0'^3 + 4[(2 - f)f - \xi^2(3 - 2f)]x_0'. \quad (4.15)$$

The general solution to this equation is given by functions which satisfy

$$\left(\frac{\partial x_0}{\partial u}\right)^2 = \frac{u^4(\xi^2 - f)}{u_h^4 f^2(1 - Cf)}, \quad (4.16)$$

where C is an integration constant.

Neglecting the perturbations δx and $\delta \mathcal{U}$, the boundary conditions (4.7) lead to the two endpoint equations

$$\left(\frac{\partial x_0}{\partial u}\right)^2 = \frac{\xi^2 - f}{f^2}, \quad (4.17a)$$

$$\left(\frac{d\mathcal{U}_0}{dt}\right)^2 = \frac{f^2(\xi^2 - f)}{\xi^2}, \quad (4.17b)$$

where all quantities are evaluated at the string endpoint. Comparing Eq. (4.17a) with Eq. (4.16), we see that the two conditions agree provided $C = 1$. In other words, the boundary condition forces the integration constant C to equal unity. Furthermore, comparing Eq. (4.17b) with Eq. (4.5b), we see that the radial motion of the string endpoint in the stationary solution coincides with that of a light-like geodesic (when ξ of the stationary solution is identified with ξ of the geodesic). Since the speed of the string endpoint necessarily equals the local speed of light, this implies that the zeroth order endpoint trajectory, given by $u = \mathcal{U}_0(t)$ and $x = \mathcal{X}_0(t) \equiv x_{\text{steady}}(t, \mathcal{U}_0(t))$, is precisely a null geodesic.

With $C = 1$, the (negative root of the) differential equation (4.16) for $x_0(u)$ becomes

$$\frac{\partial x_0}{\partial u} = -\frac{\sqrt{\xi^2 - f}}{f}. \quad (4.18)$$

(Taking the negative square root gives a solution which, for $\xi > 0$, trails the endpoint.) Substituting the steady state solution x_{steady} into Eq. (4.8) and using the above differential equation for $x_0(u)$, reveals that the steady state string solution is one whose worldsheet metric is everywhere degenerate, $\gamma = 0$. That is, x_{steady} represents a null string which is everywhere expanding at the local speed of light.

In the special case $\xi = 1$ (which will be of particular interest below), Eq. (4.18) may be integrated analytically. One finds

$$x_0(u) = \frac{u_h}{2} \left[\tan^{-1} \left(\frac{u}{u_h} \right) + \frac{1}{2} \log \left(\frac{u_h - u}{u_h + u} \right) \right]. \quad (4.19)$$

This is the well known trailing string profile of Ref. [13]. Similarly, when $\xi = 1$ the boundary condition (4.17b) may be integrated to find $\mathcal{U}_0(t)$. The solution is given implicitly by the equation

$$t - t_* = -x_0(\mathcal{U}_0) - \frac{u_h^2}{\mathcal{U}_0} + x_0(u_*) + \frac{u_h^2}{u_*}. \quad (4.20)$$

But in much of what follows it will be useful to keep ξ arbitrary.

Having found the zeroth order solution, we now turn to the first order correction which describes perturbations to a stationary null string. Linearizing Eq. (4.9) in $\delta x(t, u)$ yields the equation of motion

$$0 = \xi^2 \delta \ddot{x} + f^2 (\xi^2 - f) \delta x'' + 2\xi f \sqrt{\xi^2 - f} \delta \dot{x}' + \frac{4\xi (\xi^2 - 2f + f^2)}{u \sqrt{\xi^2 - f}} \delta \dot{x} - \frac{2f^2 (1 - 2\xi^2 + f)}{u} \delta x'. \quad (4.21)$$

A general solution to this equation can be constructed explicitly and has the form

$$\delta x(t, u) = u_h [\varphi(z(t, u)) + g(u) \psi(z(t, u))], \quad (4.22)$$

where $\varphi(z)$ and $\psi(z)$ are arbitrary functions, $g(u)$ satisfies

$$g' = \frac{u_h^3}{u^4} \sqrt{\xi^2 - f}, \quad (4.23)$$

and the function $z(u, t)$ is given by⁵

$$z(t, u) \equiv \frac{u_*}{u_h^2} [x_{\text{steady}}(t, u) - x_{\text{geo}}(u)] + z_0, \quad (4.24)$$

⁵ The overall factors of u_h , u_h^3/u^4 , and u_*/u_h^2 in Eqs. (4.22), (4.23) and (4.24) are inserted for dimensional consistency and later convenience.

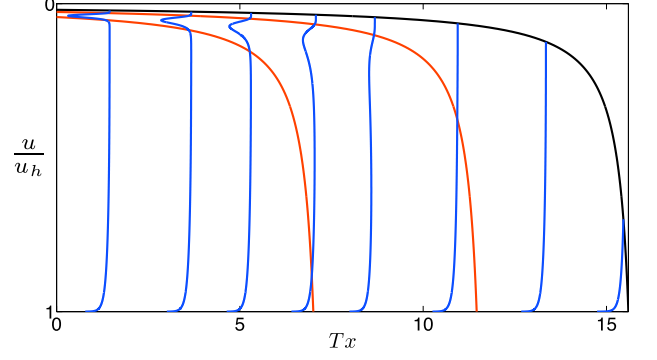


FIG. 5: The inflation of a perturbation on an expanding string. The thin blue lines show the string at eight different instants of time. The uppermost black curve shows the endpoint trajectory. The perturbation to the stationary profile is the bump initially located close to the string endpoint. For clarity, we greatly exaggerate the size of the perturbation. The two red curves are lightlike geodesics which enclose the perturbation at all times. Even though the perturbation is initially highly localized, the two geodesics which bound the perturbation rapidly separate, and correspondingly the size of the perturbation rapidly inflates as it falls into the horizon.

with z_0 an arbitrary constant. For the special case of $\xi = 1$, one has $g(u) = -u_h/u$. [Note that any constant of integration appearing in $g(u)$ can be absorbed into the definition of $\varphi(z)$.]

Using Eqs. (4.6) and (4.18), one easily finds that $z(t, u)$ is constant along null geodesics with the constant of motion ξ . Moreover, we may choose the constant z_0 such that z vanishes on the endpoint trajectory $\mathcal{U}_0(t)$.

The fact that the perturbative solution to the string equations of motion contains two arbitrary functions $\varphi(z)$ and $\psi(z)$ is to be expected. As discussed in the previous section, the required initial data for the evolution of an initially pointlike string consists of two arbitrary velocity profiles. Evidently, the information contained in the initial data gets mapped via the equations of motion onto the two functions $\varphi(z)$ and $\psi(z)$.

It is easy to understand the physical nature of the perturbations on top of the null string profile. The null string is everywhere expanding at the local speed of light. This expansion is analogous to cosmological inflation — perturbations defined on top of the null string at different points are causally disconnected and are transported along light-like geodesics. As illustrated in Fig. (5), neighboring geodesics increasingly deviate from each other. Therefore, as time progresses, the perturbations defined on top of the null string inflate to long wavelengths.

To finish the first order analysis, we need to find the correction to the endpoint trajectory. At linear order in δU and δx , the boundary conditions (4.7) yield the constraints

$$\psi(0) = 0, \quad (4.25)$$

and

$$\delta\dot{\mathcal{U}} = \frac{1}{\xi\sqrt{\xi^2 - f}} \left[(\varphi'_0 + g\psi'_0) f^2 + \frac{2\mathcal{U}_0^3 \delta\mathcal{U}}{u_h^4} (3f - 2\xi) \right], \quad (4.26)$$

where $\varphi'_0 \equiv \varphi'(0)$, $\psi'_0 \equiv \psi'(0)$, and f and g are evaluated at $\mathcal{U}_0(t)$.

1. Stopping distance

If the size of the perturbations on top of the null string solution are small, then it is easy to compute the stopping distance — the total distance Δx traveled by the string endpoint after time t_* . As the endpoint trajectories of null strings are lightlike geodesics, Δx is simply given by the total spatial distance a geodesic travels. Eq. (4.6) gives the result for lightlike geodesics,

$$\frac{dx_{\text{geo}}}{du} = \pm \frac{1}{\sqrt{\xi^2 - f(u)}}. \quad (4.27)$$

The \pm sign reflects the fact that light-like geodesics can both fall toward the horizon and shoot upwards towards the boundary. Integrating this equation will yield the total stopping distance.

Reality of Eq. (4.27) implies that $\xi^2 \geq f(u_{\min})$, where u_{\min} is the minimal radial coordinate achieved along the geodesic trajectory. We are interested in trajectories for which $u_{\min} \ll u_*$, so we require $\xi^2 \geq f(u_{\min}) \rightarrow 1$. Physically, this corresponds to geodesics which only fall in the vicinity of t_* and thereafter. This is sensible in the limit where the string creation point $u_c \rightarrow 0$, since for reasonable initial conditions any portion of the motion in which the string endpoint is moving upward toward the boundary must occur during the initial transients shortly after the creation event and well before t_* .

For geodesics which only fall, Eq. (4.27) implies that

$$\Delta x = \int_{u_*}^{u_h} \frac{du}{\sqrt{\xi^2 - f(u)}}. \quad (4.28)$$

With the restriction that $\xi \geq 1$, Δx is maximized at $\xi = 1$. To leading order in $u_*/u_h \ll 1$, evaluating the integral (4.28) gives

$$\Delta x_{\max} = \frac{u_h^2}{u_*}. \quad (4.29)$$

We must now relate the stopping distance to the quark energy at time t_* . To make this meaningful, we want to estimate the minimum amount of energy required for a quark to travel a distance Δx before thermalizing. This requires determining how the string energy scales with u_* .

The canonical momentum densities of the string are

given by

$$\pi_M^0 = -T_0 \frac{G_{MN}}{\sqrt{-\gamma}} \left[(\dot{X} \cdot X') X'^N - (X'^2) \dot{X}^N \right], \quad (4.30a)$$

$$\pi_M^1 = -T_0 \frac{G_{MN}}{\sqrt{-\gamma}} \left[(\dot{X} \cdot X') \dot{X}^N - (\dot{X}^2) X'^N \right], \quad (4.30b)$$

where $-\gamma = (\dot{X} \cdot X')^2 - \dot{X}^2 X'^2$. The energy of the string at time t_* is then given by

$$E_* = - \int_{u_*}^{u_h} du \pi_t^0. \quad (4.31)$$

The zeroth-order approximation to the string solution is a null string, for which γ vanishes. Hence, to describe a finite energy configuration, it is essential to include the perturbations to the null string profile. The determinant of the world-sheet metric will necessarily be proportional to the size of these perturbations. At linear order, and for $\xi = 1$, we have⁶

$$\gamma = \frac{2L^4}{u^4} \psi(z). \quad (4.32)$$

For a timelike worldsheet γ must be negative, and hence we must have $\psi(z) < 0$. Evaluating the string energy (4.31) to linear order in perturbations, one finds

$$E_* = \frac{\sqrt{\lambda}}{2\pi} \int_{u_*}^{u_h} \frac{du}{u^2 f} [-2\psi(z(t_*, u))]^{-1/2}. \quad (4.33)$$

This expression contains an infrared divergence near the horizon. This divergence reflects the unboundedly large amount of energy transferred to the plasma from the quark before time t_* .⁷ To extract a meaningful energy which can be associated with the quark at time t_* , we focus on the UV sensitive part of the integral (4.33). Neglecting the IR region is tantamount to cutting off the radial integral at a radial coordinate $u_{\text{IR}} < u_h$. The UV sensitive part of the string energy is the leftover part of the integral that diverges as $u_* \rightarrow 0$. This is the portion of the string energy that should be identified with the energy of a localized quark jet at time t_* .

To minimize the energy (4.33) for a given value of u_* , one wants to maximize the magnitude of the function $\psi(z)$ which characterizes the fluctuation profile. However, it is necessary to ensure that the perturbative treatment remains valid near the string endpoint — one cannot arbitrarily crank up the size of $\psi(z)$ as one must

⁶ To linear order in the size of perturbations away from the null string, the function $\varphi(z)$ appearing in Eq. (4.22) does not enter into the determinant of the worldsheet metric. In other words, perturbations in the steady state profile x_{steady} induced by $\varphi(z)$ alone preserve (to first order) the everywhere null character of the string worldsheet.

⁷ More precisely, the upper limit of the integrals (4.31) and (4.33) should not be u_h , it should be the maximal radial coordinate of any point on the string at time t_* — which rapidly approaches u_h . The contribution to the energy from the region $u \gg u_*$ reflects energy transferred to the plasma at times $t \ll t_*$.

ensure that the relations (4.13) are satisfied. More physically, we demand a well behaved solution, which is approximately a steady state solution, in the $u_* \rightarrow 0$ limit. We remind the reader that, as discussed above in Section IV A, solutions which are approximately steady state solutions are dual to long lived quarks.

At time t_* , the UV sensitive part of the string energy comes from contributions near the string endpoint. Hence, we focus our attention on the region in which $u = wu_*$ with $w = \mathcal{O}(1)$. Within this region we have

$$x_0(wu_*) = -\frac{w^3 u_*^3}{3u_h^2} + \mathcal{O}(u_*^7). \quad (4.34)$$

Then from (4.22) we see that δx will scale with the same power of u_* if

$$\phi(z) = \left(\frac{u_*}{u_h}\right)^3 \tilde{\phi}(z), \quad (4.35a)$$

$$\psi(z) = \left(\frac{u_*}{u_h}\right)^4 \tilde{\psi}(z), \quad (4.35b)$$

with $\tilde{\phi}(z)$ and $\tilde{\psi}(z)$ functions which remain bounded as $u_* \rightarrow 0$. With these scalings, a small δx relative to x_0 can always be obtained by adjusting the overall normalization of δx with a numerical factor which is independent of u_* . Similar conclusions can also be reached regarding the scaling of $\delta\mathcal{U}$ relative to that of \mathcal{U} .⁸

With the above scaling of ψ , we see that the UV sensitive part of the energy (4.33) can be written

$$E_* = \frac{u_h^2 \sqrt{\lambda}}{\pi^4 u_*^3} \frac{1}{\mathcal{C}^3}, \quad (4.36)$$

where

$$\frac{1}{\mathcal{C}^3} \equiv \frac{\pi^3}{2} \int_1^{w_{\text{IR}}} \frac{dw}{w^2} \left[-2\tilde{\psi}(z(t_*, u_* w)) \right]^{-1/2}, \quad (4.37)$$

and $w_{\text{IR}} = u_{\text{IR}}/u_*$. By the scaling relations (4.35), the constant \mathcal{C} is finite and independent of u_* in the $u_* \rightarrow 0$ limit.

After using the result (4.36) to express u_* in terms of E_* , Eq. (4.29) yields

$$\Delta x_{\text{max}}(E_*) = \frac{\mathcal{C}}{T} \left(\frac{E_*}{T\sqrt{\lambda}} \right)^{1/3}. \quad (4.38)$$

We reiterate that the $E_*^{1/3}$ scaling is the *maximum* possible power of energy consistent with the perturbative solution we have derived. In particular, it is the maximum power consistent with a string profile which is approximately a steady state profile.

⁸ From the differential equation (4.26), the scalings of φ and ψ imply $\delta\mathcal{U}$ scales like u_* . Therefore, in the $u_* \rightarrow 0$ limit the smallness of $\delta\mathcal{U}$ relative to \mathcal{U} , which is at most u_* , can always be achieved by adjusting the size of $\delta\mathcal{U}$ with a constant independent of u_* .

B. Numerical string solutions

It is instructive to complement the above analytic analysis with explicit examination of numerically computed string solutions. We wish to verify explicitly that (i) strings whose endpoints travel far in the Minkowski spatial are well approximated by null strings, (ii) the endpoint trajectories of such strings are well approximated by light-like geodesics with $\xi = 1$, and (iii) the maximum distance Δx that a string endpoint can travel scales like $E^{1/3}$. The first two points have already been demonstrated numerically in Ref. [34], but we have extended that earlier analysis by exploring a larger sample of initial conditions. This larger sample size is what allows us to address point (iii). As we are using the same numerical methods as in Ref. [34], this section closely parallels the analogous discussion there.

To gain insight into the predicted $E^{1/3}$ scaling of Δx , we solve the string equations of motion numerically for a variety of initial conditions, and plot the penetration depth as a function of energy. As discussed below, we indeed find that the scaling relation (4.38) represents an upper bound on how far a string endpoint can travel for a given initial energy. Moreover, the numerical solutions provide a direct estimate of the constant \mathcal{C} in the bound (4.38).

For reasons discussed below (and earlier in Ref. [13]), in our numerical analysis we have found it convenient to use the Polyakov string action. The Nambu-Goto action is classically equivalent to the Polyakov action

$$S_P = -\frac{T_0}{2} \int d^2\sigma \sqrt{-\eta} \eta^{ab} \partial_a X^M \partial_b X^N G_{MN}, \quad (4.39)$$

where one has introduced additional degrees of freedom in η_{ab} , the worldsheet metric. Varying the Polyakov action with respect to η_{ab} generates the constraint equation

$$\gamma_{ab} = \frac{1}{2} \eta_{ab} \eta^{cd} \gamma_{cd}. \quad (4.40)$$

This implies that

$$\sqrt{-\gamma} \gamma^{ab} = \sqrt{-\eta} \eta^{ab}, \quad (4.41)$$

so that the worldsheet metric differs from the induced metric only by a Weyl transformation,

$$\eta_{ab}(\tau, \sigma) = e^{2\omega(\tau, \sigma)} \gamma_{ab}(\tau, \sigma). \quad (4.42)$$

When Eq. (4.41) is substituted back into the Polyakov action, one recovers the Nambu-Goto action.

The equations of motion for the embedding functions X^M as well as the open string boundary conditions follow from variation of the Polyakov action with respect to the X^M . Specifically, one finds

$$\begin{aligned} \partial_a [\sqrt{-\eta} \eta^{ab} G_{MN} \partial_b X^N] \\ = \frac{1}{2} \sqrt{-\eta} \eta^{ab} \frac{\partial G_{NP}}{\partial X^M} \partial_a X^N \partial_b X^P, \end{aligned} \quad (4.43)$$

together with the boundary conditions

$$\pi_M^\sigma(\tau, \sigma^*) = 0. \quad (4.44)$$

Here $\sigma = \sigma^*$ denotes a string endpoint and π_M^σ is the canonical momentum flux on the worldsheet,

$$\pi_M^\sigma(\tau, \sigma) \equiv \frac{\delta S_P}{\delta X'^M(\tau, \sigma)} = -T_0 \sqrt{-\eta} \eta^{\sigma a} G_{MN} \partial_a X^N. \quad (4.45)$$

We can fix the coordinate parametrization (τ, σ) by choosing the worldsheet metric η_{ab} . As in Refs. [13, 34], we have found it convenient to choose η_{ab} to be of the form

$$\|\eta_{ab}\| = \begin{pmatrix} -\Sigma(x, u) & 0 \\ 0 & \Sigma(x, u)^{-1} \end{pmatrix}. \quad (4.46)$$

We refer to Σ as the stretching function, which we take to be a function of $x(\tau, \sigma)$ and $u(\tau, \sigma)$ only. The choice of the stretching function Σ is a choice of gauge. Changes in Σ lead to different embedding functions $X^M(\tau, \sigma)$, but do not affect the geometry of the target worldsheet. With a worldsheet metric of the form (4.46), the constraint equations Eq. (4.40) read

$$\dot{X} \cdot X' = 0, \quad (4.47a)$$

$$\dot{X}^2 + \Sigma^2 X'^2 = 0. \quad (4.47b)$$

Since we choose to study strings with point-like initial conditions, the σ derivatives X'^M are initially zero. Hence, we must choose initial time derivatives \dot{X}^M which are consistent with the constraint (4.47b) and the boundary condition (4.44). We may satisfy the constraint (4.47b) by fixing \dot{t} in terms of \dot{x} and \dot{u} via

$$f \dot{t}^2 = \dot{x}^2 + \frac{\dot{u}^2}{f}. \quad (4.48)$$

To satisfy the open string boundary condition (4.44) at worldsheet time $\tau = 0$, we choose \dot{x} and \dot{u} so that

$$\dot{x}'(0, \sigma^*) = \dot{u}'(0, \sigma^*) = 0. \quad (4.49)$$

The set of pointlike initial conditions then reduce to the choice of two functions \dot{x} and \dot{u} obeying Eq. (4.49), together with the initial radial coordinate u_c .

To understand why it is preferable to start from the Polyakov action instead of the Nambu-Goto action when solving numerically for the string dynamics, note that the equations of motion (4.43) contain relative factors of $(-\eta)^{-1}$ between different terms. Consequently, the string equations become singular whenever $\sqrt{-\eta} \rightarrow 0$. If we choose the worldsheet metric to be the induced metric, which is equivalent to starting from the Nambu-Goto action, then the equations of motion become singular as any part of the string approaches a lightlike configuration. This always happens at late times as the string accelerates toward the black brane. By using the Polyakov form of the string action, and exploiting the freedom to choose

a worldsheet metric of the form (4.46), we may rescale the worldsheet metric so that the equations of motion remain well-behaved everywhere on the worldsheet.

The energy of the string is a conserved quantity and can be computed from the data defining the initial conditions. With

$$\pi_t^\tau(\tau, \sigma) = \frac{\delta S_P}{\delta \dot{t}(\tau, \sigma)} \quad (4.50)$$

denoting the conserved canonical energy density, the total string energy is given by

$$E_{\text{string}} = - \int_0^\pi d\sigma \pi_t^\tau(0, \sigma). \quad (4.51)$$

Expressing this more explicitly in terms of the initial data, one finds that

$$E_{\text{string}} = \frac{\sqrt{\lambda}}{2\pi} \frac{f(u_c)}{\Sigma(x_c, u_c) u_c^2} \int_0^\pi d\sigma \dot{t}(0, \sigma). \quad (4.52)$$

1. Initial conditions and numerical results

We consider a two-parameter family of initial conditions. Inspired by the strings studied in Ref. [34], we choose

$$\dot{x}(0, \sigma) = A u_c \cos \sigma, \quad (4.53a)$$

$$\dot{u}(0, \sigma) = u_c \sqrt{f(u_c)} (1 - \cos 2\sigma), \quad (4.53b)$$

and also take $x_c = 0$. As $u_c \rightarrow 0$ and $A u_c \rightarrow \infty$, these initial conditions generate strings whose endpoints travel arbitrarily far in the Minkowski spatial directions before falling into the black hole. Moreover, since $\dot{x}(0, \sigma)$ is antisymmetric about $\sigma = \pi/2$ while $\dot{u}(0, \sigma)$ is symmetric, these strings are symmetric about $x = 0$ at all times. These states therefore have zero total spatial momentum, but each half of the string has an energy and momentum that scale linearly with A for large A .

As in Refs. [13, 34], we choose a stretching function so that gradients of the embedding functions are small at all times during the string's evolution. We found by trial and error that stretching functions of the form

$$\Sigma(x, u) = \left[1 + \left(\frac{x}{\pi T} \right)^2 \right]^m \left(\frac{1 - u/u_h}{1 - u_c/u_h} \right) \left(\frac{u_c}{u} \right)^2. \quad (4.54)$$

were adequate to generate long-lived strings with a variety of initial conditions. In this work, the free parameter m was usually chosen to be 0.02.

In terms of the initial conditions (4.53) and the stretching function (4.54), the string's energy evaluates to

$$E_{\text{string}} = \frac{\sqrt{\lambda}}{2\pi} \frac{\sqrt{f(u_c)}}{u_c} \int_0^\pi d\sigma \sqrt{A^2 \cos^2 \sigma + (1 - \cos 2\sigma)^2}. \quad (4.55)$$

Because the string corresponds to a quark-antiquark pair in the dual field theory, E_{string} should be regarded as

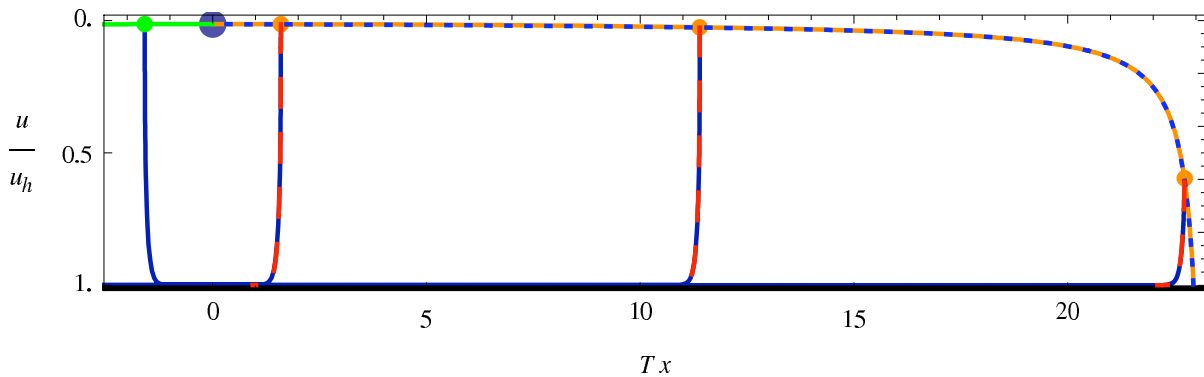


FIG. 6: A plot of a numerically computed string at three different times, overlain with the analytic null string approximation (4.12). The string was created at a point at time $t = 0$ with the initial conditions (4.53), for $u_c = 0.014 u_h$ and $A = 2400$. The corresponding energy $E = E_{\text{string}}/2 \simeq 85700 \sqrt{\lambda} T$. The numerical string, shown as the solid blue curve, is plotted at successive times $t_1 = 1.6/T$, $t_2 = 11.4/T$, and $t_3 = 22.8/T$, and the corresponding null string, shown as the dashed red curve, is plotted at the same times. The solid green and orange curves represent the numerically computed endpoint trajectories, and the overlain dashed blue curve shows the geodesic fit to the endpoint trajectory with geodesic parameter $\xi = 1$. The null string approximation agrees very well with the numeric string configuration at times $t \gtrsim$ a few u_h , and the null geodesic curve likewise tracks the endpoint trajectory very accurately.

twice the initial energy of a single quark. We emphasize that our strings are symmetric about $x = 0$ so that each half-string is approximately dual to a single dressed quark. In the following we therefore use

$$E \equiv \frac{1}{2} E_{\text{string}}, \quad (4.56)$$

when discussing the dynamics of a single string endpoint.

As in Refs. [13, 34], we used the Mathematica routine `NDSolve` to integrate the string equations of motion (4.43) numerically. We chose the parameters A and u_c in our initial conditions (4.53) from the intervals

$$A \in [1000, 9000], \quad (4.57a)$$

$$\frac{u_c}{u_h} \in [0.00867, 0.019]. \quad (4.57b)$$

This generates half-strings with energies in the interval

$$\frac{E}{\sqrt{\lambda} T} \in [26316, 519031], \quad (4.58)$$

allowing us to study states with energies much larger than the characteristic scale $\sqrt{\lambda} T$ (while simultaneously achieving high numerical precision).

Our data runs stepped through this parameter space by fixing u_c and then generating strings for many values of A . As a result, we were able to generate over a thousand string worldsheets and measure the associated stopping distances and energies. Our data are summarized in Fig. 1. Each distinct line of data points in the plot comes from a single choice for u_c .

2. Comparison to the approximate string solution

Fig. 6 displays a typical numerically generated string at three different coordinate times. On top of the numerical string profiles, we also plot the null string (4.12) with

$\xi = 1$. Also shown in the figure are the endpoint trajectories overlain with the corresponding null geodesic with $\xi = 1$. As is evident from the figure, the null string provides an excellent approximation to the numerical string profiles for times t which are a few u_h or larger, and the difference between the actual endpoint trajectory and the null geodesic approximation is imperceptible.

To further elucidate the quality of the geodesic approximation to the endpoint trajectory, we have computed the quantity

$$\Xi(t) \equiv f(\mathcal{U}(t)) (d\mathcal{X}/dt)^{-1}, \quad (4.59)$$

where $\mathcal{X}(t)$ is the \hat{x} -coordinate of the string endpoint. From Eq. (4.5a), one sees that for a geodesic Ξ is constant and equal to ξ . Over the course of the trajectory of the numerical string shown in Fig. 6, Ξ equals 1 to within one part in 10^6 , which is the limit of our numerical precision. Therefore, the endpoint path for this string is very well approximated by a $\xi = 1$ geodesic. We have verified similar results for many different sets of initial conditions which correspond to long lived quarks.

3. Maximum penetration depth

Our exploration of a wide range of initial conditions produced the data for penetration depths shown in Fig. 1. All our data are consistent with the bound

$$\Delta x_{\text{max}}(E) = \frac{0.526}{T} \left(\frac{E}{T\sqrt{\lambda}} \right)^{1/3}, \quad (4.60)$$

which explicitly confirms the $E^{1/3}$ scaling of the penetration depth derived in Section IV A. More generally, our numerical results clearly confirm the validity of the

asymptotic analysis leading to the approximate string solution presented in Section IV A.

It is instructive to estimate the maximum value of \mathcal{C} based on the perturbative analysis presented in Section IV A. Clearly, from Eq. (4.37) one sees that \mathcal{C} is maximized when the quantity $\tilde{\psi}(z)$ is maximized. However, the validity of the null string approximation presented in Section IV A required $|\tilde{\psi}(z)| \ll 1$. For $\tilde{\psi}(z) \sim 1$ the integration appearing in Eq. (4.37) is order one. Furthermore, the value of \mathcal{C} only depends on the cube root of the integral, so \mathcal{C} is rather insensitive to its precise value. Therefore, in order to get a crude estimate on the value of \mathcal{C} we set the integral appearing in Eq. (4.37) equal to one. We therefore arrive at the estimate

$$\mathcal{C} \sim \frac{\sqrt{2}}{\pi} \approx 0.45. \quad (4.61)$$

This is remarkably close to the numerically determined value of 0.526

In addition to the sampling of point-like initial conditions yielding the data shown in Fig. 1, we have also studied more complicated initial conditions describing strings which are not point-like at $t = 0$. The results obtained for these initial conditions also demonstrated the $E^{1/3}$ scaling relation of Eq. (4.38), but generally yielded a slightly smaller value of \mathcal{C} . All of our numerical results are consistent with the value for \mathcal{C} determined from the data shown in Fig. 1, namely $\mathcal{C} = 0.526$. However, we emphasize that this value, extracted from a finite sampling of initial conditions, is a lower bound on the true value of \mathcal{C} . It is possible that a wider set of initial conditions will yield a larger value for \mathcal{C} , although because of the close agreement with the estimate obtained in Eq. (4.61), we doubt that the true value is significantly greater than 0.526.

V. DISCUSSION

A. Energy loss rate

As Fig. 1 makes apparent, propagating light quarks in strongly-coupled $\mathcal{N} = 4$ plasma do not have a unique stopping distance for a given energy. This result should not be surprising. Knowledge of the total energy (and momentum) of a quark-antiquark state is far from a complete specification of the initial state. The form of the disturbance in the gauge field (and other $\mathcal{N} = 4$ SYM fields) will affect the subsequent dynamics. In the dual description, this additional information is encoded in the profile of the string connecting the quark and antiquark. Nevertheless, there is a rather simple characterization of the maximum penetration distance of a quark, scaling with energy as $E^{1/3}$.

An interesting quantity to consider is the instantaneous energy loss rate of a light quark. From the $\Delta x \sim E^{1/3}$ scaling of the penetration depth, one might expect that for light quarks the rate of energy loss per distance

traveled, dE/dx (which essentially coincides with dE/dt while the excitation is a good quasiparticle), would scale like $E^{2/3}$. This expectation turns out to be incorrect, as we now discuss.

Let $f_{\text{drag}}^\mu(t) = dp^\mu/dt$ denote the four momentum lost by the quark per unit time. The long distance hydrodynamic perturbation in the SYM stress tensor $T_{\text{hydro}}^{\mu\nu}$ is determined by the hydrodynamic constituent relations together with the energy-momentum conservation relation [31],

$$\partial_\mu T_{\text{hydro}}^{\mu\nu} = F^\nu, \quad (5.1)$$

with $F^\mu(t, \mathbf{x}) = -f_{\text{drag}}^\mu(t) \delta^{(3)}(\mathbf{x} - \mathbf{x}_{\text{quark}}(t))$ the force-density (acting on the plasma) and $\mathbf{x}_{\text{quark}}(t)$ the quark's trajectory.

As long as the quark's baryon density is well-localized in space, the energy loss rate may be determined by computing the energy flux through a sphere S_R of radius R which encloses (nearly) all of the quark's baryon density. It is this energy flux which enters in the force density of Eq. (5.1). As $1/T$ sets the length scale on which a hydrodynamic description of the stress tensor perturbation becomes valid [31], it is natural to take $R \sim 1/T$. The precise value chosen for R is irrelevant — during times in which the quark is a well defined quasiparticle, its baryon density is localized over a scale $\ll 1/T$ while the distance traveled by the localized baryon density distribution is $\gg 1/T$.

Using the dual gravitational description, one may compute the energy flux through S_R by solving the gravitational bulk-to-boundary problem. Specifically, one solves Einstein's equations for the perturbation in the $5d$ geometry due to the presence of the string and then, by analyzing the near boundary behavior of the metric perturbation [31, 41, 42], extracts the change in the SYM stress tensor and uses this result to evaluate the energy flux through S_R . This procedure was carried out for heavy quarks moving at constant velocity in Refs. [30, 31, 32, 33]. Carrying out the corresponding analysis for our non-stationary light quark worldsheets is computationally demanding and will be left for future work. However, there is a simple way of extracting the energy loss rate from the string profile itself. The energy of a string is a conserved quantity. The high energy density near the string endpoint should, as discussed in Section III, be regarded as the energy of the quark. This energy is transported down the string by an energy flux π_t^1 [cf. Eq. (4.30b)] towards the event horizon. This energy flux corresponds to energy transferred from the quark to the plasma. Via the holographic bulk-to-boundary mapping, this conserved flux is mapped onto the energy flux through S_R in the dual field theory. Without solving the bulk-to-boundary problem explicitly, one does not know a-priori precisely how to relate the bulk position (u, t) at which one evaluates the energy flux down the string to a corresponding time and radius R of an energy flux measurement in the field theory. However, as long as the quark energy loss rate is changing sufficiently slowly,

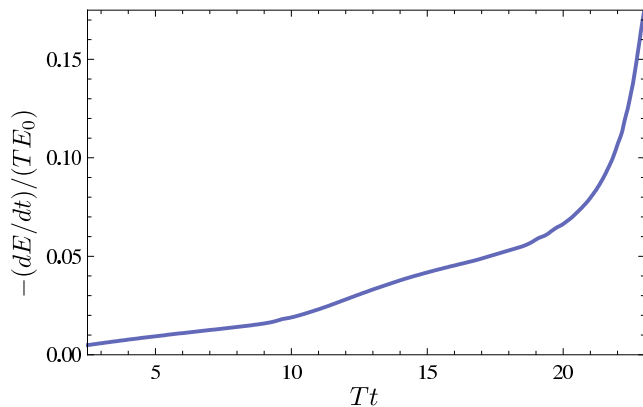


FIG. 7: The instantaneous energy loss rate, dE/dt , of a highly energetic quark, normalized by its initial energy E_0 . Instead of decreasing with time, as might have been expected, the light quark energy loss rate actually increases. At times near the thermalization time, which for this particular example is $t_{\text{therm}} \sim 24/T$, the instantaneous energy loss rate grows like $dE/dt \sim 1/\sqrt{t_{\text{therm}} - t}$.

retardation effects in the gravitational bulk-to-boundary problem can be neglected and the energy flux through S_R should be well approximated by evaluating the energy flux down the string at a spatial distance $\sim R$ from the string endpoint.

In Fig. 7, we plot the energy flux flowing down the numerically generated string shown in Fig. 6, evaluated at a distance of $1.75/(\pi T)$ from the string endpoint. For this particular string, the string endpoint approaches the event horizon at a time $t \sim 24/T$, which should be regarded as the thermalization time t_{therm} of the light quark. As the string endpoint approaches the event horizon, the baryon density induced on the boundary rapidly spreads out and diffuses [34]. In the gravitational description, this is due to the strong gravitational redshift incurred on the electric field sourced by the string endpoints as they approach the horizon.⁹ As is evident from Fig. 7, the energy flux down the string does not decrease in a power-law fashion as a naive $E^{2/3}$ scaling of dE/dt would suggest, but rather increases monotonically until the thermalization time!

We stress that the precise form of the energy flux down the string is sensitive to the initial conditions used to create the string. This is easy to understand from the approximate analytic string solutions discussed in Section IV A. These approximate solutions, which correspond to long-lived quarks, are perturbations of null

strings. The energy flux diverges for a null string. The finite flux of the complete solution is determined by the function $\psi(z(t, u))$ [defined in Eq. (4.22)] which characterizes the perturbation $\delta x(t, u)$ on the null string. This function is not universal, and depends on the initial conditions used to create the string.

However, the late time behavior of the instantaneous energy flux is universal. As is evident from Fig. 7, near the thermalization time the energy flux down the string dramatically increases. This may be understood from our approximate string solutions. The energy flux down the string scales like $(-\gamma)^{-1/2}$ where γ is the determinant of the worldsheet metric. For strings which are small perturbations of null strings, Eq. (4.32) shows γ is proportional to the function $\psi(z(t, u))$ characterizing the perturbations. Near the thermalization time $t_{\text{therm}} = u_h^2/u_*$ and at a radial coordinate u corresponding to a fixed distance $\sim 1/T$ from the string endpoint, the function $z(t, u)$ behaves like

$$z(t, u) = \frac{t - t_{\text{therm}}}{u_*} + \mathcal{O}(u_*/u_h), \quad (5.2)$$

and hence becomes very small as $t \rightarrow t_{\text{therm}}$. By the open string boundary conditions (4.7) and (4.25), the function $\psi(z)$ must vanish at the string endpoint which, as discussed in Section IV A corresponds to $z = 0$. Finiteness of the string energy (4.33) requires that $\psi'(0)$ be non-zero. Consequently, near the endpoint one may approximate $\psi(z) \approx \psi'(0)z$. Neglecting the $\mathcal{O}(u_*/u_h)$ corrections in Eq. (5.2), one finds

$$\pi_t^1 \sim \frac{1}{\sqrt{t_{\text{therm}} - t}}. \quad (5.3)$$

We have numerically confirmed the above scaling in the data shown in Fig. 7.

The late-time behavior (5.3) implies that after traveling substantial distances through the plasma, the thermalization of light quarks ends with an “explosive” transfer of energy to the plasma. This behavior is qualitatively similar to the energy loss rate of a fast charged particle moving through ordinary matter, where the energy loss rate has a pronounced peak (known as a “Bragg peak”) near the stopping point. This peak in the energy loss rate has its origin in the energy dependence of cross sections, which increase with decreasing energy due to the conformal nature of Coulomb interactions.

In the gravitational description, the scaling (5.3) becomes valid when the string endpoint starts to fall toward the horizon (*i.e.*, when $dU/d\mathcal{X}$ ceases to be small compared to one). As shown in Fig. 6, this happens relatively abruptly, so we expect the creation of large amounts of gravitational radiation to propagate to the boundary and induce a large perturbation in the SYM stress tensor corresponding to this final burst of energy. However, we emphasize that because the energy flux flowing down the string is changing rapidly at late times, retardation effects in the gravitational bulk-to-boundary problem cannot be neglected, implying that the result (5.3) for the

⁹ More precisely, as the string endpoints approach the horizon, the strong gravitational field of the black hole pulls the electric field lines, which are sourced by the string endpoints, towards the horizon. This results in the spreading out of the electric field lines and hence a spreading out of the induced baryon density on the boundary.

energy flux down the string cannot be directly equated with the field theory energy flux through a sphere S_R . It would, of course, be interesting to compute directly the energy flux in the plasma produced by the light quark jet as it thermalizes. Evaluation of the required bulk-to-boundary problem is currently in progress.

It is interesting to speculate on the implications of our results for heavy ion collisions. Hard partons produced in the early stages of heavy ion collisions can traverse the resulting fireball and deposit energy and momentum into the medium. If the partons are moving supersonically, their hydrodynamic wake will contain a Mach cone whose propagation can influence the distribution of particles associated with a jet. If the hard parton under consideration is a very massive quark with mass m , the results of Ref. [13] predict an energy loss rate of the form $dE/dx = dp/dt = -\mu p$ where, for strongly coupled SYM, $\mu = \frac{\pi}{2} \sqrt{\lambda} T^2/m$. Therefore, the energy loss rate falls exponentially with time — heavy quarks in strongly coupled SYM lose the bulk of their energy in the early portions of their trajectories. The resulting sound waves, whose amplitudes will be largest at early times, may traverse much of the fireball before freezeout occurs. Consequently, sound waves produced by heavy quarks may be quite sensitive to medium effects and may experience substantial attenuation before freezeout.

At least for strongly coupled SYM, the situation for light quarks is qualitatively different. As we have demonstrated in Fig. 7, light quarks lose the bulk of their energy in the latter stages of their trajectories. The resulting hydrodynamic wake will therefore have less time to attenuate and diffuse than is the case for heavy quarks. Moreover, because the light quark energy loss rate increases with time, we expect the amplitude of the corresponding wake to also increase with time. Because of this, we expect the spectrum and distribution of particles produced by light quark jets to be qualitatively different from the behavior of heavy quark jets.

B. Fluctuations

Throughout our analysis, we have treated the string dynamics classically. This approximation is valid in the limit of large 't Hooft coupling λ . More precisely, a classical treatment is valid in the limit that $\lambda \rightarrow \infty$ with $E/\sqrt{\lambda}T$ finite and fixed. (Recall that the string energy automatically scales like $\sqrt{\lambda}$.) However, one would also like to understand when the classical analysis can be trusted if λ is large but fixed. To determine this, one should compute the size of quantum fluctuations around the classical string profile and compare the size of the fluctuations to the classical result. Natural specific quantities to consider are the fluctuations Δp in the quark momentum \mathbf{p} . These fluctuations are defined by the variances

$$(\Delta p_i(t))^2 = \langle p_i(t)^2 \rangle - \langle p_i(t) \rangle^2. \quad (5.4)$$

If $\Delta \mathbf{p}$ is not small compared to \mathbf{p} , then the reliability of the classical calculation is questionable.

Formally, the mean momentum \mathbf{p} and the connected correlator defining $(\Delta p)^2$ are both $O(\sqrt{\lambda})$. Consequently $|\Delta p/p| = O(\lambda^{-1/4})$ and vanishes as $\lambda \rightarrow \infty$. However, for large but fixed λ the energy (and time) dependence of $|\Delta p/p|$ can be important. To see this, consider the case of fluctuations in the momentum of a heavy quark. Mean square fluctuations in the longitudinal and transverse components of the quark's momentum grow with time t as [15, 20]

$$(\Delta p_L)^2 \sim \sqrt{\lambda} \gamma^{5/2} T^3 t, \quad (5.5a)$$

and

$$(\Delta p_T)^2 \sim \sqrt{\lambda} \gamma^{1/2} T^3 t, \quad (5.5b)$$

respectively, where $\gamma \equiv 1/\sqrt{1-v^2}$ and v is the heavy quark velocity. Therefore, with large but fixed λ , the relative size of fluctuations, $\Delta p/p$, becomes arbitrarily large both at sufficiently late times and (for longitudinal fluctuations) in the ultra-relativistic limit.

To estimate the size of quantum fluctuations in the light quark's momentum, we will use the above results for heavy quarks as a rough guide. This is not unreasonable as the trailing string profile used to compute the above momentum fluctuations coincides, in the $v \rightarrow 1$ limit, with the ($\xi = 1$) null string derived in Section IV A. However, care must be taken — quantum fluctuations on top of the null string, which is a degenerate solution to the classical equations of motion, diverge. This is immediately apparent in the formulas (5.5) which blow up as $v \rightarrow 1$. To estimate the momentum fluctuations for light quarks using these results, we must be able to associate the heavy quark velocity v (which is always less than 1) with the size of the *classical* perturbations δx [defined in Eq. (4.11)] to the null string profile. To do so, we simply note that the trailing string profile for a heavy quark with velocity v coincides with the null string profile (which is the $v \rightarrow 1$ limit) up to $O(1-v^2)$ corrections. Therefore, for the purpose of a rough estimate, we identify $1-v^2$ with the size of classical perturbations on top of the null string. As discussed in Section IV A 1, if at time t_* the radial coordinate of the string is u_* , then the largest¹⁰ the perturbations to the null string can be is $O(u_*^3/u_h^3)$. With the identification $1-v^2 \iff O(u_*^3/u_h^3)$, we have

$$(\Delta p_L)^2 \sim \left(\frac{u_h}{u_*} \right)^{15/4} \sqrt{\lambda} T^3 t. \quad (5.6)$$

During the portion of the quark's trajectory when it is a well defined quasi-particle its momentum, by construc-

¹⁰ Strictly speaking, in Section IV A 1 we argued that δx can be no larger than u_*^3/u_h^3 only in the vicinity of the string endpoint. However, via the inflationary behavior of perturbations defined on top of the null string (as shown in Fig. 5), when $t - t_* = O(1/T)$ the perturbation in the string profile will be determined by the near endpoint perturbations at time $t = t_*$.

tion, is large and scales as $p \sim \sqrt{\lambda} u_h^2 / u_*^3$. We therefore arrive at the estimate

$$\frac{\Delta p}{p} \sim \left(\frac{u_*}{u_h} \right)^{9/8} \frac{\sqrt{T} t}{\lambda^{1/4}}. \quad (5.7)$$

In the limit $u_*/u_h \ll 1$ (*i.e.* the high energy limit) we see that the size of quantum fluctuations are small relative to the classical prediction for the momentum. But for fixed values of u_* and λ , the \sqrt{t} growth of the result (5.7) suggests there will be a time when quantum fluctuations become large. However, for the light quarks discussed in this paper, the quarks only exist as well defined quasiparticles up until the thermalization time t_{therm} . As discussed in Section IV A, in terms of u_* the thermalization time is simply $t_{\text{therm}} = u_h^2 / u_*$. Evaluated at this time, Eq. (5.7) implies that quantum fluctuations are suppressed by a relative factor of $(u_*/u_h)^{5/8} / \lambda^{1/4}$. This is reassuring.

C. Pair creation, string fragmentation and finite N_c

In addition to large λ , we have also assumed from the outset that N_c has been sent to infinity. This limit is what justifies the neglect of quantum fluctuations in the background AdS-BH geometry. At finite N_c , string fragmentation, backreaction of the string on both the geometry and the $D7$ brane embedding, and backreaction of the brane on the geometry also have to be addressed.

Energetically, our string is unstable to breaking into many tiny pieces. This corresponds to quark-antiquark pair creation in the dual field theory. The small string coupling $g_s \sim 1/N_c$ suppresses the amplitude for a string to break. Correspondingly, the rate of the string decay process is suppressed by $1/N_c^2$, and hence the time scale for string fragmentation is, at large N_c , parametrically larger than any of the time scales considered in this work.

Alternatively, the process of string fragmentation can also be described from the point of view of the $D7$ brane worldvolume as the spreading of a narrow flux tube, the original fundamental string, into more and more widely dispersed flux on the brane. In terms of the underlying string theory, the quanta of the worldvolume gauge field are little pieces of open string, so a uniform flux on the worldvolume is the same as a coherent cloud of little string pieces. Thinking of the dynamical instability of our string as a result of breaking into many pieces, or due to spreading into dispersed flux on the brane, are just two different descriptions of one and the same process which is suppressed at large N_c .

Large N_c is also what justifies the neglect of backreaction of the $D7$ brane on the background geometry, as well as the backreaction of the string on the $D7$ brane embedding and on the geometry. Note that, as far as large N_c counting is concerned, the gravitational action scales as N_c^2 , the action for the brane embedding and the worldvolume gauge field scales as N_c , and the Nambu-Goto action describing the worldsheet of the string is of

order 1. (In addition the three actions scale with the 't Hooft coupling as 1, λ and $\sqrt{\lambda}$, but for now it is sufficient to focus on the N_c counting.) The brane is very heavy compared to the string, but still has a small tension in Planck units. Consequently, it is consistent to embed the brane in a fixed background geometry and then consider a string ending on the brane, without computing the $\mathcal{O}(1/N_c)$ suppressed deformation of the brane which will be induced by the string.

The issue of backreaction becomes more subtle when one solves for the linearized response of the metric in response to the string in order to determine the boundary stress tensor. The order N_c^0 stress energy of the string generates an order $1/N_c^2$ correction to the metric (since the $5d$ gravitational constant scales as $1/N_c^2$). Consequently, when evaluating the variation of the on-shell gravitational action, the perturbation in the geometry due to the presence of the string produces an order one contribution to the expectation value of the stress tensor.

In addition to the string itself, another potential source for the stress tensor is the gauge field living on the brane which is sourced by the string endpoint. The $O(1)$ charge from the string endpoint gives rise to an order $1/N_c$ gauge field on the brane [as the gauge coupling on the brane is $\mathcal{O}(1/N_c)$]. Combining this with the overall N_c of the brane action would appear to give another order one source in the bulk, and hence another order one contribution to the expectation value of the stress tensor out on the boundary.

However, it is important to note that the leading \mathcal{A}_M dependent term in the brane stress tensor is quadratic in the worldvolume gauge field, so that the order $1/N_c$ gauge field on the brane only produces a stress-tensor contribution of order $1/N_c$. This conclusion is altered if there is an order one background electric field on the worldvolume (as in the original dragging string solution of Ref [13]). In this case there are contributions to the brane stress tensor linear in the gauge field sourced by the string, which consequently give rise to an order one contribution to the stress tensor. Similar terms also arise if one studies finite, non-zero mass quarks where an order one background embedding scalar is turned on. Both of these contributions would need to be included if one wanted to generalize the stress-energy wake calculations of Refs. [30, 31, 32, 33] to finite mass quarks.

D. Weak versus strong coupling

It is natural to ask how the $E^{1/3}$ scaling of the penetration depth in the strongly coupled limit compares with the analogous result for weakly coupled plasmas. When the 't Hooft coupling λ (at scales ranging from the temperature T to the projectile energy E) is small, the energy loss of a high energy parton moving through the plasma is dominated by near-collinear bremsstrahlung processes. The rate for an energetic parton (with energy $E \gg T$) to radiate a gluon which carries away

an $O(1)$ fraction of its energy, while interacting with a typical gauge field fluctuation in the plasma, scales as $\lambda^2 T / \sqrt{E/T}$ [43, 44, 45, 46, 47], up to factors depending logarithmically on the energy, which we ignore throughout this discussion. Therefore, the average distance an energetic parton travels between emission events is $\Delta x_{\text{rad}}(E) \sim \sqrt{E/T} / (\lambda^2 T)$. The square root dependence on energy is due to LPM suppression, which is a consequence of multiple scattering during the formation time of a radiated gluon.

Imagine creating a very energetic quark in a localized wave-packet with mean momentum \mathbf{p} , and then measuring, at some later time, the total energy or baryon number contained in a co-moving sphere of size $R \sim 1/T \gg 1/|\mathbf{p}|$ surrounding the wave-packet. The opening angle in near-collinear bremsstrahlung emission is parametrically small, $\Delta\theta \sim \sqrt{\lambda} (T/E)^{3/4}$. Therefore, the direction of the leading parton is almost unchanged by these bremsstrahlung emissions. Since the speeds of ultrarelativistic excitations differ negligibly from the speed of light, this implies that all the partons produced by a cascade of near-collinear emissions have almost identical velocities. Consequently, near-collinear bremsstrahlung emissions do not significantly degrade the energy, or baryon number, contained in the co-moving sphere. As far as gauge-invariant measurements of energy or momentum are concerned, the entire collection of near-collinear partons behaves like a single collective excitation whose energy and momentum is nearly constant.

This effective “quasi-particle” picture remains valid until the typical energy of the partons produced by the cascade ceases to be large compared to T . The typical penetration depth will equal the radiation length $\Delta x_{\text{rad}}(E)$ summed over the number of levels of showering which are required to degrade the typical parton energy from E down to $\approx T$. Since every emission transfers an $O(1)$ fraction of energy to the emitted gluon, and every produced parton continues to shower, the typical energy of partons produced by a cascade with k levels of showering will be of order E/c^k for some $c \approx 2$. Therefore, the number of showerings required to thermalize an extremely energetic parton grows only logarithmically with energy, and the total penetration depth differs from the radiation length for the first emission only by an $O(1)$ factor. The net result is that the penetration depth $\Delta x(E)$ in a weakly coupled non-Abelian plasma behaves as $\sqrt{E/T} / (\lambda^2 T)$ times factors depending only logarithmically on E/T .

Presumably, there is a smooth interpolation from weak to strong coupling in $\mathcal{N}=4$ SYM. At intermediate couplings, the maximum penetration depth may be proportional to $E^{\nu(\lambda)}$, with an exponent $\nu(\lambda)$ which varies smoothly from $1/2$ as $\lambda \rightarrow 0$ to $1/3$ as $\lambda \rightarrow \infty$. Alternatively, the correct form might be a sum of two distinct contributions, $T \Delta x = A(\lambda) (E/T)^{1/2} + B(\lambda) (E/T)^{1/3}$, with $A(\lambda) = \mathcal{O}(\lambda^{-2})$ and $B(\lambda) = o(\lambda)$ as $\lambda \rightarrow 0$, and $B(\lambda) = \mathcal{O}(\lambda^{-1/6})$ and $A(\lambda) = o(\lambda^{-1/6})$ as $\lambda \rightarrow \infty$. Subleading corrections to the weak-coupling energy loss rate

which are suppressed by powers of the 't Hooft coupling are not known, and would be challenging to calculate. And subleading strong-coupling corrections, suppressed by inverse powers of λ , are also unknown. Consequently, there is no way, at present, to determine a preferred interpolating form.

E. Relation to other work

In Ref. [35], where the $E^{1/3}$ scaling was first proposed, various guesses for the analog of \mathcal{C} were given based on different assumptions. The authors of this work were interested in calculating the penetration depth of a gluon, whose dual description was conjectured to be a folded string. The relevant string configuration was assumed to be given by a portion of the stationary trailing string profile of Ref. [13], with the string (at any instant of time) coming up from the horizon, reaching a sharp hairpin at some radial coordinate $u_*(t)$, and then retracing the same path back down to the horizon.

The authors of Ref. [35] estimated the penetration depth of a gluon by assuming that the hairpin in the string falls into the horizon along a lightlike geodesic. Without solving the string equations of motion, the parameters of the geodesic were estimated in terms of u_* and v . By relating the these parameters to the string's energy, the authors of Ref. [35] argued that the maximum penetration depth should scale like

$$\Delta x_{GGPR} = \frac{\mathcal{C}_{GGPR}}{T} \left(\frac{E_*}{2T\sqrt{\lambda}} \right)^{1/3}. \quad (5.8)$$

The constant \mathcal{C}_{GGPR} was estimated to be between 0.35 and 0.41.

While we have found that the endpoint trajectories of strings corresponding to long lived quarks do follow lightlike geodesics (to quite high accuracy), the relationship between the parameters of the geodesic and the energy of string are rather different than that presented in Ref. [35]. In contrast to the treatment of Ref. [35], where the string energy was assumed to be well-described by $E_{GGPR} \sim \sqrt{\lambda} / (u_* \sqrt{1-v^2})$, the energy of the strings considered in this paper scale as $\sqrt{\lambda} u_h^2 / u_*^3$ and the strings themselves are approximately null — this latter fact completely fixes the corresponding geodesic parameter ξ in terms of the initial string profile via the equations of motion.

Despite these differences, it may be of interest to compare the penetration depth of a gluon estimated in Ref. [35] with the result for a light quark found in this paper. In doing so, it is natural to replace $E_*/2 \rightarrow E_*$, in Eq. (5.8) when converting from a folded string modeling a gluon to an open string describing a quark. With this change, one may simply compare \mathcal{C}_{GGPR} to our measured value of $\mathcal{C} = 0.526$. Our result is larger than the estimates of Ref. [35] by 30–50%.

The $E^{1/3}$ scaling of the penetration depth has also appeared in Ref. [36], which discussed the dynamics of jet-

like configurations in the bulk gauge field dual to the R -current in strongly coupled SYM. The coefficient of the scaling relation was not calculated in this work. However, the coefficient characterizing R -current jets necessarily differs from our result in Eq. (4.60), since the gravitational interactions of the $5d$ gauge field dual to the boundary R -current are independent of λ (at leading order in the strong coupling limit).

We conclude our discussion by summarizing the physics which distinguishes light quark energy loss from that of heavy quarks. A comprehensive numerical study of heavy quark evolution has been performed in Ref. [29]. Let us compare and contrast the behavior of heavy and light quarks. The penetration distance in both cases is non-universal for the same reason: the quark's evolution depends upon the initial gauge field. After several units of inverse temperature, the dual string in either case becomes well approximated by small fluctuations on top of an analytic solution. As long as the quark is ultra-relativistic (regardless of its mass), the appropriate analytic string solutions are null strings, and the energy flux flowing down the string is entirely determined by the non-universal small fluctuations. However, when a heavy quark has lost a sufficient amount of energy, its dual string profile will be well approximated by the non-null $v < c$ solutions obtained in Ref. [13]. Thereafter, the heavy quark energy loss rate will be insensitive to fluctuations away from the analytic string profile, and the energy loss rate will simply be proportional to the quark's momentum. In contrast, the light quark energy loss rate remains sensitively dependent on fluctuations during its entire trajectory. This is a consequence of the fact massless quarks are always ultra-relativistic, so their dual string profile is nearly null at all times. Consequently, the energy loss rate profile of a light quark remains sensitive to the initial conditions for an arbitrar-

ily long period until thermalization.

VI. CONCLUSIONS

Using gauge/gravity duality, we have studied the penetration depth of an energetic light quark moving through a strongly coupled $\mathcal{N}=4$ SYM plasma. An analytic asymptotic analysis shows that, for quarks which travel long distances through the plasma, the worldsheet of the dual string description nearly coincides with that of null string. Both the analytic analysis, and explicit numerical computations, show that for a given quark energy E , the maximum penetration depth $\Delta x_{\max}(E)$ scales as $E^{1/3}$. Based on numerical results from a wide sampling of initial conditions, we find $\Delta x_{\max}(E) = (\mathcal{C}/T) (E/T\sqrt{\lambda})^{1/3}$ with $\mathcal{C} \approx 0.5$. We also find that the instantaneous energy loss rate of a light quark is not universal. However, independent of initial conditions, we find that the energy loss rate grows rapidly as the thermalization time is approached. Consequently, the thermalization of light quarks in strongly coupled $\mathcal{N}=4$ super Yang-Mills ends with an “explosive” burst of energy transfer to the plasma.

Acknowledgments

We thank J. Casalderrey-Solana, E. Iancu, H. Liu, G. Moore and D. Teaney for useful comments and discussions. This work was supported in part by the U.S. Department of Energy under Grant No. DE-FG02-96ER40956. P.C. and L.G.Y. thank the Kavli Institute for Theoretical Physics for its hospitality during the completion of key parts of this paper.

-
- [1] E. Shuryak, “Why does the quark gluon plasma at RHIC behave as a nearly ideal fluid?,” *Prog. Part. Nucl. Phys.* **53** (2004) 273–303, [arXiv:hep-ph/0312227](#).
 - [2] E. V. Shuryak, “What RHIC experiments and theory tell us about properties of quark-gluon plasma?,” *Nucl. Phys.* **A750** (2005) 64–83, [arXiv:hep-ph/0405066](#).
 - [3] M. J. Leitch, “Latest results on the hot-dense partonic matter at RHIC,” *Eur. Phys. J.* **A31** (2007) 868–874, [arXiv:nucl-ex/0610015](#).
 - [4] J. Casalderrey-Solana, E. V. Shuryak, and D. Teaney, “Hydrodynamic flow from fast particles,” [arXiv:hep-ph/0602183](#).
 - [5] J. M. Maldacena, “The large N limit of superconformal field theories and supergravity,” *Adv. Theor. Math. Phys.* **2** (1998) 231–252, [arXiv:hep-th/9711200](#).
 - [6] E. Witten, “Anti-de Sitter space and holography,” *Adv. Theor. Math. Phys.* **2** (1998) 253–291, [arXiv:hep-th/9802150](#).
 - [7] S. S. Gubser, I. R. Klebanov, and A. M. Polyakov, “Gauge theory correlators from non-critical string theory,” *Phys. Lett.* **B428** (1998) 105–114, [arXiv:hep-th/9802109](#).
 - [8] O. Aharony, S. S. Gubser, J. M. Maldacena, H. Ooguri, and Y. Oz, “Large N field theories, string theory and gravity,” *Phys. Rept.* **323** (2000) 183–386, [arXiv:hep-th/9905111](#).
 - [9] S. Caron-Huot, P. Kovtun, G. D. Moore, A. Starinets, and L. G. Yaffe, “Photon and dilepton production in supersymmetric Yang-Mills plasma,” *JHEP* **12** (2006) 015, [arXiv:hep-th/0607237](#).
 - [10] S. C. Huot, S. Jeon, and G. D. Moore, “Shear viscosity in weakly coupled $\mathcal{N}=4$ super Yang-Mills theory compared to QCD,” *Phys. Rev. Lett.* **98** (2007) 172303, [arXiv:hep-ph/0608062](#).
 - [11] P. M. Chesler and A. Vuorinen, “Heavy flavor diffusion in weakly coupled $\mathcal{N}=4$ super Yang-Mills theory,” *JHEP* **11** (2006) 037, [arXiv:hep-ph/0607148](#).
 - [12] P. Kovtun, D. T. Son, and A. O. Starinets, “Viscosity in strongly interacting quantum field theories from black hole physics,” *Phys. Rev. Lett.* **94** (2005) 111601,

- arXiv:hep-th/0405231.
- [13] C. P. Herzog, A. Karch, P. Kovtun, C. Kozcaz, and L. G. Yaffe, “Energy loss of a heavy quark moving through $\mathcal{N}=4$ supersymmetric Yang-Mills plasma,” *JHEP* **07** (2006) 013, arXiv:hep-th/0605158.
 - [14] J. Casalderrey-Solana and D. Teaney, “Heavy quark diffusion in strongly coupled $\mathcal{N}=4$ Yang Mills,” *Phys. Rev.* **D74** (2006) 085012, arXiv:hep-ph/0605199.
 - [15] S. S. Gubser, “Momentum fluctuations of heavy quarks in the gauge-string duality,” *Nucl. Phys.* **B790** (2008) 175–199, arXiv:hep-th/0612143.
 - [16] S. S. Gubser, “Comparing the drag force on heavy quarks in $\mathcal{N}=4$ super-Yang-Mills theory and QCD,” *Phys. Rev.* **D76** (2007) 126003, arXiv:hep-th/0611272.
 - [17] H. Liu, K. Rajagopal, and U. A. Wiedemann, “Calculating the jet quenching parameter from AdS/CFT,” *Phys. Rev. Lett.* **97** (2006) 182301, arXiv:hep-ph/0605178.
 - [18] E. Shuryak, “The conical flow from quenched jets in sQGP,” *Nucl. Phys.* **A783** (2007) 31–38, arXiv:nucl-th/0609013.
 - [19] S. Lin and E. Shuryak, “Toward the AdS/CFT gravity dual for High Energy Collisions: I. Falling into the AdS,” *Phys. Rev.* **D77** (2008) 085013, arXiv:hep-ph/0610168.
 - [20] J. Casalderrey-Solana and D. Teaney, “Transverse momentum broadening of a fast quark in a $\mathcal{N}=4$ Yang-Mills plasma,” *JHEP* **04** (2007) 039, arXiv:hep-th/0701123.
 - [21] S. Lin and E. Shuryak, “Stress tensor of static dipoles in strongly coupled $\mathcal{N}=4$ gauge theory,” *Phys. Rev.* **D76** (2007) 085014, arXiv:0707.3135 [hep-th].
 - [22] S. Lin and E. Shuryak, “Toward the AdS/CFT Gravity Dual for High Energy Collisions: II. The Stress Tensor on the Boundary,” *Phys. Rev.* **D77** (2008) 085014, arXiv:0711.0736 [hep-th].
 - [23] Y. Hatta, E. Iancu, and A. H. Mueller, “Deep inelastic scattering off a $\mathcal{N}=4$ SYM plasma at strong coupling,” *JHEP* **01** (2008) 063, arXiv:0710.5297 [hep-th].
 - [24] K. Dusling *et al.*, “Quarkonium transport in thermal AdS/CFT,” arXiv:0808.0957 [hep-th].
 - [25] H. Liu, K. Rajagopal, and Y. Shi, “Robustness and Infrared Sensitivity of Various Observables in the Application of AdS/CFT to Heavy Ion Collisions,” *JHEP* **08** (2008) 048, arXiv:0803.3214 [hep-ph].
 - [26] G. Policastro, D. T. Son, and A. O. Starinets, “The shear viscosity of strongly coupled $\mathcal{N}=4$ supersymmetric Yang-Mills plasma,” *Phys. Rev. Lett.* **87** (2001) 081601, arXiv:hep-th/0104066.
 - [27] M. Luzum and P. Romatschke, “Conformal relativistic viscous hydrodynamics: Applications to RHIC,” *Phys. Rev.* **C78** (2008) 034915, arXiv:0804.4015 [nucl-th].
 - [28] S. S. Gubser, “Drag force in AdS/CFT,” *Phys. Rev.* **D74** (2006) 126005, arXiv:hep-th/0605182.
 - [29] M. Chernicoff and A. Guijosa, “Acceleration, energy loss and screening in strongly- coupled gauge theories,” *JHEP* **06** (2008) 005, arXiv:0803.3070 [hep-th].
 - [30] P. M. Chesler and L. G. Yaffe, “The wake of a quark moving through a strongly-coupled $\mathcal{N}=4$ supersymmetric Yang-Mills plasma,” *Phys. Rev. Lett.* **99** (2007) 152001, arXiv:0706.0368 [hep-th].
 - [31] P. M. Chesler and L. G. Yaffe, “The stress-energy tensor of a quark moving through a strongly-coupled $\mathcal{N}=4$ supersymmetric Yang-Mills plasma: comparing hydrodynamics and AdS/CFT,” *Phys. Rev.* **D78** (2008) 045013, arXiv:0712.0050 [hep-th].
 - [32] S. S. Gubser, S. S. Pufu, and A. Yarom, “Energy disturbances due to a moving quark from gauge-string duality,” *JHEP* **09** (2007) 108, arXiv:0706.0213 [hep-th].
 - [33] S. S. Gubser, S. S. Pufu, and A. Yarom, “Sonic booms and diffusion wakes generated by a heavy quark in thermal AdS/CFT,” *Phys. Rev. Lett.* **100** (2008) 012301, arXiv:0706.4307 [hep-th].
 - [34] P. M. Chesler, K. Jensen, and A. Karch, “Jets in strongly-coupled $\mathcal{N}=4$ super Yang-Mills theory,” arXiv:0804.3110 [hep-th].
 - [35] S. S. Gubser, D. R. Gulotta, S. S. Pufu, and F. D. Rocha, “Gluon energy loss in the gauge-string duality,” arXiv:0803.1470 [hep-th].
 - [36] Y. Hatta, E. Iancu, and A. H. Mueller, “Jet evolution in the $\mathcal{N}=4$ SYM plasma at strong coupling,” *JHEP* **05** (2008) 037, arXiv:0803.2481 [hep-th].
 - [37] D. M. Hofman and J. Maldacena, “Conformal collider physics: Energy and charge correlations,” *JHEP* **05** (2008) 012, arXiv:0803.1467 [hep-th].
 - [38] A. Karch and E. Katz, “Adding flavor to AdS/CFT,” *JHEP* **06** (2002) 043, arXiv:hep-th/0205236.
 - [39] P. K. Kovtun and A. O. Starinets, “Quasinormal modes and holography,” *Phys. Rev.* **D72** (2005) 086009, arXiv:hep-th/0506184.
 - [40] J. D. Brown and J. York, James W., “Quasilocal energy and conserved charges derived from the gravitational action,” *Phys. Rev.* **D47** (1993) 1407–1419, arXiv:gr-qc/9209012.
 - [41] K. Skenderis, “Asymptotically anti-de Sitter spacetimes and their stress energy tensor,” *Int. J. Mod. Phys.* **A16** (2001) 740–749, arXiv:hep-th/0010138.
 - [42] J. J. Friess, S. S. Gubser, G. Michalogiorgakis, and S. S. Pufu, “The stress tensor of a quark moving through $\mathcal{N}=4$ thermal plasma,” *Phys. Rev.* **D75** (2007) 106003, arXiv:hep-th/0607022.
 - [43] R. Baier, Y. L. Dokshitzer, A. H. Mueller, S. Peigne, and D. Schiff, “Radiative energy loss of high energy quarks and gluons in a finite-volume quark-gluon plasma,” *Nucl. Phys.* **B483** (1997) 291–320, arXiv:hep-ph/9607355.
 - [44] R. Baier, Y. L. Dokshitzer, A. H. Mueller, and D. Schiff, “Medium-induced radiative energy loss: Equivalence between the BDMPS and Zakharov formalisms,” *Nucl. Phys.* **B531** (1998) 403–425, arXiv:hep-ph/9804212.
 - [45] B. G. Zakharov, “Fully quantum treatment of the Landau-Pomeranchuk-Migdal effect in QED and QCD,” *JETP Lett.* **63** (1996) 952–957, arXiv:hep-ph/9607440.
 - [46] S. Jeon and G. D. Moore, “Energy loss of leading partons in a thermal QCD medium,” *Phys. Rev.* **C71** (2005) 034901, arXiv:hep-ph/0309332.
 - [47] P. Arnold and C. Dogan, “QCD splitting/joining functions at finite temperature in the deep LPM regime,” arXiv:0804.3359 [hep-ph].